

POLITECNICO OF TURIN

**Master's Degree in**  
**Automotive Engineering**  
Master's Degree Thesis

**Design of engine components with thermoplastic composite material:  
Connecting Rod**



**Relator/Correlator**

prof. Paolo Baldissera  
prof. Cristiana Delprete

**Candidate**

Matteo Conese

A.A. 2018/2019



## ***Abstract***

In the last decades, the automotive sector has experienced great progress in reached velocity, comfort or security. These new conditions, together with a stricter legislation about the global pollution, lead to new requirements that the fabricants must face in the market. One of the fields where the companies are spending their effort and time is the engine efficiency and fuel economy. In this optimization process, FEM (Finite Element Method) is the most used tool, being the weight component reduction one of the most important aspect to decrease the fuel consumption.

In this project, a new configuration for the connecting rod has been analysed in terms of material stress and weight reduction. This study was performed in parallel with one about the wrist pin, following the same considerations in FEM tuning and physical simplified model. Due to the material characteristics, the thermal stress wasn't considered.

Focusing on the innovation desire, the component has been designed in composite material, in particular carbon fibre. It is the best material to obtain a significant weight reduction. However, the aim of this study was also to obtain a better stress distribution inside the component. For this reason, it was designed a new way to impose the preload to the cap, avoiding the classical bolts. The main dimensions of the rod were taken from the Fiat Fire 1.4 8V engine, while the final geometry considered both the space inside the engine and the production process.

To perform this FEM study, different programs have been used. First, the geometry was drawn using Solidworks of Dassault Systemes and then it has been reduced in forms of surfaces, has been cleaned, prepared and meshed with the software HyperMesh of Altair. The simulations were performed with the solver Optistruct. Finally, the results have been analysed using HyperView.

Keywords: Hypermesh, Optistruct, FEM, Connecting rod, Composite material, Carbon Fibre



4.2	FEM Results .....	28
4.2.1	Tensile Load .....	29
4.2.2	Buckling Load .....	46
4.2.3	Bending Load .....	54
4.3	Future development .....	62
4.4	Alternative model.....	63
I.	Bibliography.....	64

## **List of Figures**

Figure 2-1 Reduced Connecting Rod.....	6
Figure 2-2 Centred Crank Mechanism Layout .....	7
Figure 2-3 Crank Masses and Centrifugal Forces.....	8
Figure 2-4 Tensile Load .....	9
Figure 2-5 Buckling Load .....	10
Figure 2-6 Bending Load .....	11
Figure 3-1 Text Editor for PCOMPLS .....	15
Figure 3-2 Connecting Rod with Threaded Inserts .....	16
Figure 3-3 Transversal Holes Model .....	17
Figure 3-4 Optimization Parameters .....	17
Figure 3-5 Axial Holes Model .....	18
Figure 3-6 Main Dimensions .....	18
Figure 3-7 Layered Model.....	19
Figure 3-8 Model Mesh.....	19
Figure 3-9 Material Organization.....	19
Figure 3-10 Contact Surfaces .....	20
Figure 3-11 Loadsteps .....	21
Figure 3-12 Tsai-Wu Ellipse.....	24
Figure 4-1 Alternating Force: Steel vs Composite .....	25
Figure 4-2 Torque Comparison .....	26
Figure 4-3 Engine Block Forces .....	27
Figure 4-4 Principal Stress Directions .....	28
Figure 4-5 Traction Load .....	29
Figure 4-6 Preload Constraints .....	29
Figure 4-7 Preload: Gap Opening.....	30
Figure 4-8 Preload: Contact Status .....	31
Figure 4-9 Preload: Displacement.....	32
Figure 4-10 Preload: Principal Stress Direction 1 .....	33
Figure 4-11 Preload: Principal Stress Direction 2 .....	34
Figure 4-12 Preload: Principal Stress Direction 3 .....	35
Figure 4-13 Preload: Max Shear .....	36
Figure 4-14 Traction Loadstep Constraints.....	37
Figure 4-15 Traction: Gap Opening.....	38
Figure 4-16 Traction: Contact Status .....	39
Figure 4-17 Traction: Deformation .....	40
Figure 4-18 Traction: Enlarged Deformation.....	41
Figure 4-19 Traction: P1.....	42
Figure 4-20 Traction: P2.....	43
Figure 4-21 Traction: P3.....	44
Figure 4-22 Traction: Max Shear.....	45
Figure 4-23 Buckling Load.....	46

Figure 4-24 Compression: Gap Opening.....	46
Figure 4-25 Compression: Contact Status .....	47
Figure 4-26 Compression: Displacement.....	48
Figure 4-27 Compression: Enlarged Displacement.....	49
Figure 4-28 Compression: P1 .....	50
Figure 4-29 Compression: P2 .....	51
Figure 4-30 Compression: P3 .....	52
Figure 4-31 Compression: Max Shear .....	53
Figure 4-32 Whiplash Load .....	54
Figure 4-33 Whiplash: Gap Opening.....	54
Figure 4-34 Whiplash: Contact Status .....	55
Figure 4-35 Whiplash: Displacement.....	56
Figure 4-36 Whiplash: Enlarged Deformation .....	57
Figure 4-37 Whiplash: P1 .....	58
Figure 4-38 Whiplash: P2 .....	59
Figure 4-39 Whiplash: P3 .....	60
Figure 4-40 Whiplash: Max Shear.....	61
Figure 4-41 Example of Layer Diversification .....	62
Figure 4-42 Alternative Model.....	63

## ***List of Tables***

Table 1-1 PEI-AS4 Mechanical Properties.....	3
Table 2-1 Geometrical Parameters.....	5
Table 2-2 Reduced Connecting Rod.....	6
Table 2-3 G Distance .....	12
Table 2-4 Rod Masses .....	12
Table 2-5 Wrist Pin Masses.....	12
Table 3-1 PCOMPLS Format.....	14
Table 3-2 PCOMPLS Details.....	15
Table 4-1 Mechanical Results .....	25
Table 4-2 Max Force Values.....	26
Table 4-3 Centrifugal Force Values .....	26
Table 4-4 Force Reductions .....	27
Table 4-5 Max Stress.....	28

## ***List of Equations***

Equation 1-1 Shear Modulus .....	3
Equation 2-1 Geometrical Ratio .....	5
Equation 2-2 Piston Surface.....	5
Equation 2-3 Reduced Conrod Masses.....	6
Equation 2-4 Alternating Mass .....	7
Equation 2-5 Alternating Inertial Force .....	7
Equation 2-6 Maximum Rotational Speed.....	7
Equation 2-7 Crank Masses.....	8
Equation 2-8 Centrifugal Force .....	8
Equation 2-9 Angular Acceleration.....	11
Equation 2-10 Max Distributed Load.....	11
Equation 2-11 Cross-section Rod Area .....	11
Equation 2-12 Equivalent Whiplash Load.....	11
Equation 3-1 Ply Thickness Evaluation .....	15
Equation 3-2 Tsai-Wu Formula .....	22
Equation 3-3 Tsai-Wu Reduced.....	22
Equation 3-4 Tsai-Wu Coefficients .....	23
Equation 3-5 2-D Tsai-Wu Formula.....	23
Equation 3-6 F12 Coefficient .....	23
Equation 3-7 Failure Locus.....	23
Equation 3-8 Empirical F12 .....	23
Equation 4-1 Single Crank Mechanism Torque.....	26
Equation 4-2 Resultant Force on Crank Mechanism .....	26
Equation 4-3 Engine Block Forces.....	27

# **1 Introduction**

## **1.1 General introduction**

Since its origin, the automotive industry is in continuous growth. New customers' needs and stricter norms that affect the sector, force the companies to develop and improve new technologies and studies to be competitive.

The car is the most popular land transport system, used widely all over the world. For this reason, regulations focus in this sector to reduce the environment contamination and to improve the passenger safety and comfort. The international institutions impose new norms in the field of emissions that are more restrict, and this makes the fabricants of the automotive sector to adapt to the new rules. To obtain a reduction of the harmful substances emitted to the atmosphere, the companies are always focused in designing new and more efficient propulsive systems and advanced components to save energy.

In the recent decades, the focus in optimizing the engine efficiency has grown due to the importance of reducing the consumption of the vehicle through the reduction of the weight. The weight of the engine parts studied in this case (connecting rod and wrist pin), compared to the whole car weight, is not so relevant in percentage. But their weight reduction becomes very important if we consider the reduction in stress and vibrations transmitted toward the other elements involved in the engine operation. As consequence of the reduced stresses, the geometry of lots of part can be redesigned, saving weight. Additionally, forces and vibrations induced by the engine operation affect the comfort and the noise perceived by the passengers, rising the quality level of the whole car.

The FEM (Finite Element Method) simulations are a type of analysis more and more used. This method allows studying many different conditions with a software that solves the equations of the material and therefore predict how the model behaves with those conditions in the real world. The FEM analysis for composite material is still in development, with tools that can be sometimes tricky to be used, especially with a geometry far from the laminate shape.

After this type of FEM studies, the next step that follows usually in the market is to perform experimental test in a real engine on the test-bench, to prove the results obtained in a computer. Obviously, the final part of the process is to jump to a real road and drive the car, testing its behaviour in a circuit.

## 1.2 State of Art

The connecting rod is a component which is usually made with steel, but the choice of the material can be affected depending on the purpose of the engine.

Two aspects are mainly considered: the overall mass and strength of the connecting rod and the manufacturing process together with the procedure to obtain the face junction between cap and head of the big eye.

Considering connecting rods with the face junction obtained with machining:

- **Ductile and malleable cast irons and C-treated steels**, that require low cost technologies and then are used for high production series of medium stressed engines.
- **Hardened alloy steels** (e.g. 30NiCrMo12) that require hot forging procedures (expensive) and then are preferred for high stressed engines.
- **Ti-alloy** (e.g. Ti6Al4V), especially for racing engines. This material as the advantage to be lighter than steel, keeping the same traction strength. The disadvantage is a minor yield strength.
- **Al-alloy**, for low stressed engines only.

Considering connecting rods with the face junction obtained by brittle fracture:

- **Malleable cast irons** with specific heat treatment
- **Steels with high carbon content** (e.g. C70)
- **Micro-alloyed steels** (e.g. 36MnVS4)

In innovative research field connecting rods in sintered steel with metal matrix composite, Al-alloy with carbon fibre, and high-performance thermoplastic material (e.g. PEEK) are also investigated

### 1.3 Composite Materials

A composite material is a material formed by combining two or more materials with significant differences in physical or chemical properties. In the engineering field there are many types of composite materials. This thesis is based on the Laminated Composites, which are materials made up of any number of layered materials, of the same or different orientation, bonded together with a matrix material.

The choice for the work has fallen on a UD composite material, PEI-AS4. This material is the most suitable since its properties are very good in the interested directions and at high temperatures (almost 150° C). This allows us to use it not only for the connecting rod, which is essentially loaded in one direction (the connecting rod direction itself), but also for the wrist pin.

The mechanical properties of the material are shown in the table:

<b>Young Modulus</b>	<b>E<sub>11</sub></b>	128700 MPa
	<b>E<sub>22</sub></b>	7600 MPa
	<b>E<sub>33</sub></b>	7600 MPa
<b>Shear Modulus</b>	<b>G<sub>12</sub></b>	4800 MPa
	<b>G<sub>13</sub></b>	4800 MPa
	<b>G<sub>23</sub></b>	2968,75 MPa
<b>Maximum longitudinal stress</b>	<b>F<sub>1t</sub></b>	2176 MPa
<b>Maximum transversal stress</b>	<b>F<sub>2t</sub></b>	46,7 MPa
<b>Maximum shear stress</b>	<b>F<sub>6</sub></b>	140 MPa
<b>Material Density</b>	<b>ρ</b>	1,55 g/cm <sup>3</sup>
<b>Poisson coefficient</b>	<b>ν<sub>12</sub></b>	0.28
	<b>ν<sub>23</sub></b>	0.28
<b>Filling percentage</b>	<b>V<sub>f</sub></b>	55%

Table 1-1 PEI-AS4 Mechanical Properties

In the table is also showed the value of filling percentage, which represent the amount of fibres in percentage with respect to the matrix material. Higher **V<sub>f</sub>** can be achieved, but values above 50-55% lead to considerably reduction of the laminate's mechanical properties.

The values in the Table 1-1 are related each other accordingly to that equation:

$$G_{ij} = \frac{E_{ii}}{2(1 + \nu_{ij})}$$

Equation 1-1 Shear Modulus

### **1.3.1 Why using composite materials?**

The material properties of the composites can be engineered both for the application requirements or, as in this study case, for different layering options. Composite materials property can be imparted giving them great advantage when compared with traditional homogeneous materials like steel or aluminium. Finally, composites have increased strength to weight ratios in use cases against isotropic metals.

For these reasons, applications like aerospace components, where the weight is a decisive factor, can benefit tremendously with the usage of composite materials.

Drawbacks:

- Higher cost
- Limited supply of raw materials
- Complex manufacturing needs

Considering the automotive field, an engine is subjected to high loads deriving from the combustion and the inertial forces of the components. In our model, the original engine was endowed with steel connecting rod and wrist pin. Analysing the resultant force acting on the engine block with all steel components, it is possible to notice that the value roam around 24 KN. Just by substituting the steel connecting rod and the wrist pin with those of composites, the reduction on the resultant force is about the 22% (18,5 KN).

### **1.3.2 Why using orthotropic material?**

Orthotropic materials' properties are the same in each of three orthogonal planes at a given point within a body. Thus, the material properties are dependent on orientation at a specified point within the body.

The next paragraph will show the steps used for the calculation of the forces and of the involved masses.

## 2 Connecting Rod Analysis

The connecting rod is the component that changes the reciprocating motion of the piston in the rotating motion of the crankshaft and it consists of a stem and two ends. The small eye is the housing of the bushing and of the pin. The pin connects the piston to the connecting rod. The small eye is integral to the stem. Instead, the big eye is composed by two elements: the head, integral to the stem, and the cap, connected to the head by bolts or screws. Cap and head form the housing of the bushing inserted between the crank and the connecting rod.

As a first analysis, it is considered a standard engine made of steel/cast iron. Then the analysis will be modified introducing the values for the new material. That will cause a change in the values of the masses and so of the alternating and centrifugal forces acting on the engine.

### 2.1 Geometrical Parameters

First, all the geometrical parameters of the engine are determined. Using the CAD file, it is possible to extract all the values:

<b>Crank Radius</b>	<b>r = 42 mm</b>
<b>Connecting Road</b>	<b>l = 128,95 mm</b>
<b>Piston Stroke</b>	<b>L = 84 mm</b>
<b>Piston Bore</b>	<b>B = 72 mm</b>

Table 2-1 Geometrical Parameters

From which it's possible to evaluate the values for:

- Geometrical Ratio  $\lambda$ :

$$\lambda = \frac{r}{l} = \frac{42}{128,95} = 0,325707639$$

Equation 2-1 Geometrical Ratio

This value will be used to calculate the alternating forces.

- Piston Surface  $S$ :

$$S = \pi \frac{B^2}{4} = \pi \frac{72^2}{4} = 4071,504079 \text{ mm}^2$$

Equation 2-2 Piston Surface

These values are geometrical characteristics of the engine and they are obviously valid both for original connecting rod and for the composite one.

## 2.2 Equivalent Connecting Rod

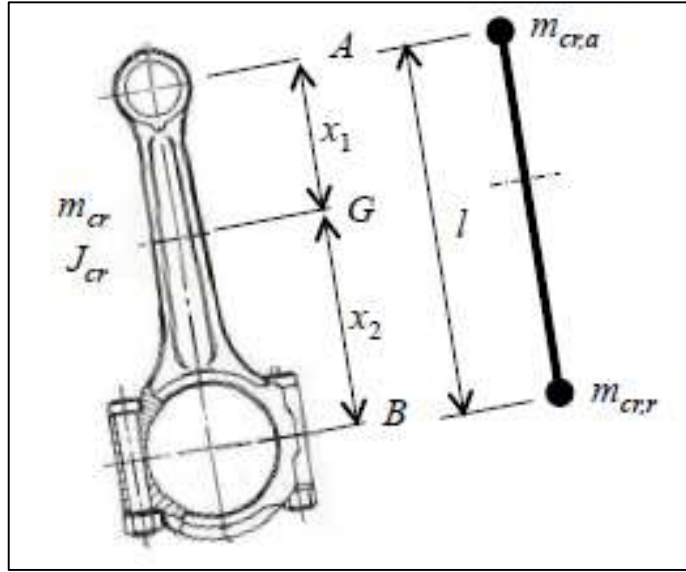


Figure 2-1 Reduced Connecting Rod

Considering the Figure 2-1, the next step consists in reducing the connecting rod to an equivalent one, where the position of the centre of gravity (G) and the mass of the connecting rod were taken from the CAD file.

<b>Connecting Rod Mass</b>	$m_{cr} = 428g$
<b>Small Eye to G</b>	$x_1 = 93,96mm$
<b>Big Eye to G Distance</b>	$x_2 = 34,99mm$

Table 2-2 Reduced Connecting Rod

The equivalent model is necessary because the alternating force are due to the mass of the piston, the pin and the upper part of the rod. This part of the rod mass,  $m_{cr,a}$ , is assumed to be in the small eye, while the other part of the rod mass,  $m_{cr,r}$ , is assumed to be in the big eye, contributing to the centrifugal force.

So:

$$\begin{cases} m_{cr,a} + m_{cr,r} = m_{cr} \\ m_{cr,a}x_1 = m_{cr,r}x_2 \\ m_{cr,a}x_1^2 + m_{cr,r}x_2^2 + J_0 = J_{cr} \end{cases} \rightarrow \begin{cases} m_{cr,r} = \frac{x_1}{x_1 + x_2} m_{cr} = 311,8641g \\ m_{cr,a} = m_{cr} - m_{cr,r} = 116,1359g \end{cases}$$

Equation 2-3 Reduced Conrod Masses

Note:  $J_0 \approx - (0.01 - 0.03)m_{cr,tot} \frac{r^2}{\lambda^2}$ , is always negative and it must be added to the moment of inertia of the connecting rod, to guarantee the conservation of the total moment of inertia.



## 2.4 Evaluation of the Centrifugal Force (at max rotational speed $n = 6250\text{rpm}$ )

Still considering the centred crank mechanism layout (Figure 2-2) and the Figure 2-3, all the bodies involved in the rotating motion of mass  $m_r$  must be considered located at the crank radius.

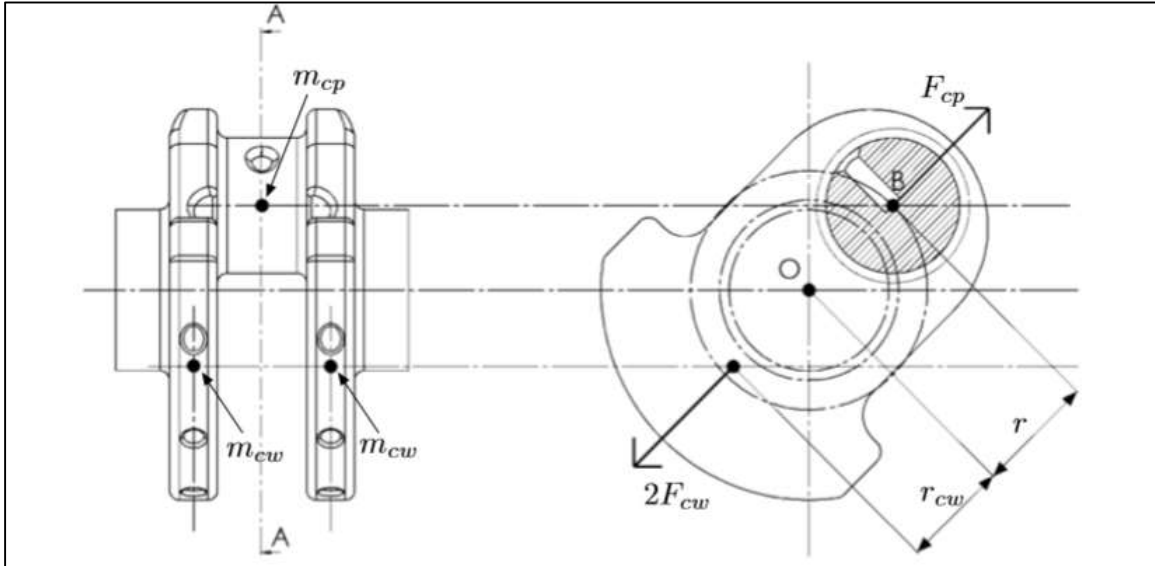


Figure 2-3 Crank Masses and Centrifugal Forces

$$\begin{cases} m_r = m_{cp} + 2m_{cw,red} + m_{cr,r} = 233,61g + 2 * 120,42g + 311,86g = 786,32g & (1) \\ m_{cw,red} = m_{cw} \frac{r_{cw}}{r} = 934,9g * \frac{5,41mm}{42mm} = 120,42g & (2) \end{cases}$$

Equation 2-7 Crank Masses

Note: The crank web mass  $m_{cw}$  is generally placed at a distance  $r_{cw}$  with respect the crank axis: it is then necessary to reduce this mass to the crank radius by imposing the equality of static moments (equation (2) in Equation 2-7).

Considering  $\omega$  in Equation 2-6, the centrifugal force is:

$$F_\omega = m_r r \omega^2$$

Equation 2-8 Centrifugal Force

Note: The values of the force will be shown later, compared with the composite case.

## 2.5 Load Conditions

Loads acting on the connecting rod are mainly due to the gas pressure and the inertial forces. Even if load conditions change during the engine cycle, to simplify the problem only two situations are considered:

- Starting condition, that considers the gas action (at the maximum torque) and neglects the inertial contribution (to maximize the compressive force)
- Operating condition at maximum engine spin speed, that neglects the gas action to maximize the inertial effect, obtaining the maximum tensile force at TDC

Usually, the first attempt analytical design of the connecting rod provides some steps:

- the first step is defining the cross-section area of the stem: the maximum compressive force is compared to the admissible stress of the chosen material and the area is evaluated
- the second step is verifying that the previous computed area satisfies the strength condition under tensile load.
- As third step, the cross-section shape has to be defined and in order to do that the buckling elastic instability condition is considered.

However, in this project, these steps have not been followed. Starting from the original shape, it was tried to maintain similar encumbrances. This was necessary to avoid interferences between the connecting rod, the piston and the crankcase.

### 2.5.1 Tensile load

The tensile load is due to the inertial forces which are evaluated at TDC, at the end of the exhaust stroke and at the maximum spin speed.

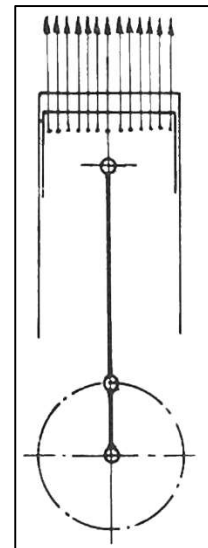


Figure 2-4 Tensile Load

### 2.5.2 Buckling Load

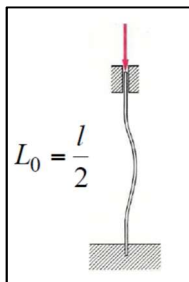
The buckling load is due to the compressive force generated by the gas expansion when the piston is at TDC or by the inertial force when the piston is at BDC.

The maximum of those two compressive forces, in the two worst cases respectively of starting or maximum speed, is the input for the buckling validation.

The buckling planes are two, with different constraints schematization in the small and big eye:

- **zy plane** (lateral plane containing the wrist pin axis)

Note: the free length  $L_0$  of this beam model is equal to the half distance between the centre of the small eye and the centre of the big eye, that is the half-length  $l/2$  of the connecting rod.



- **xy plane** (frontal plane perpendicular to the wrist pin axis)

Note: the free length  $L_0$  of this beam model is equal to the distance between the centre of the small eye and the centre of the big eye, that is the length  $l$  of the connecting rod.

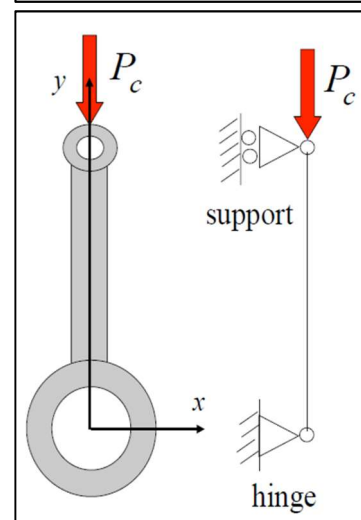
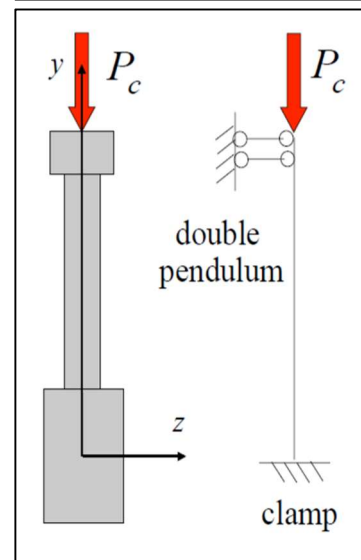
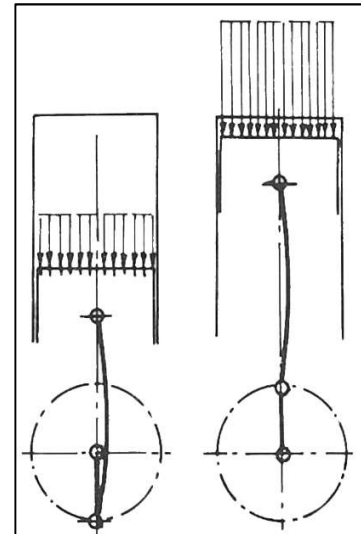
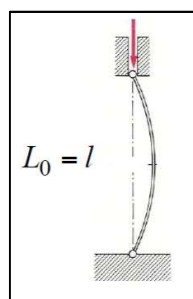


Figure 2-5 Buckling Load

Since the model in the frontal xy plane has a free length  $L_0$  higher than the model in the lateral zy plane, the model in the frontal xy plane is the most dangerous in term of elastic instability.

### 2.5.3 Bending Load

The main bending load is due to the whiplash, resulting from the acceleration distribution that the connecting rod undergoes during its roto-translational motion.

The angular acceleration of the connecting rod has a triangular distribution with null value at the centre of the small eye and maximum value  $\omega^2 r$  at the centre of the big eye.

From the crank mechanism analysis, the maximum angular acceleration of the connecting rod computed with crank angle  $\theta = 90^\circ$ , is:

$$\dot{\omega}_{cr,max} = \frac{\omega^2 \lambda}{\sqrt{1 - \lambda^2}}$$

Equation 2-9 Angular Acceleration

Or in equivalence, the connecting rod can be modelled as a beam, with constant cross section, loaded by the following triangular load distribution:

$$q_{max} = \frac{\omega^2 \lambda}{\sqrt{1 - \lambda^2}} \rho A_{cr} l = 27317,5 \text{ kg/s}^2$$

Equation 2-10 Max Distributed Load

$$\text{with } A_{cr} = 926.17 \text{ mm}^2$$

Equation 2-11 Cross-section Rod Area

$$Q = q_{max} \left( \frac{l}{2} \right) = 1762 \text{ N}$$

Equation 2-12 Equivalent Whiplash Load

An additional bending load can be due to the seizure of the bushing in the small eye and/or in the big eye, but it was neglected in this analysis.

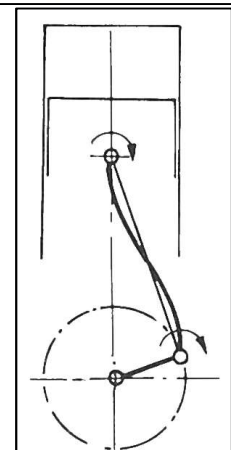
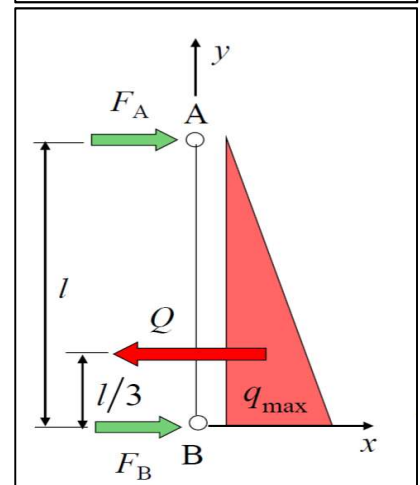
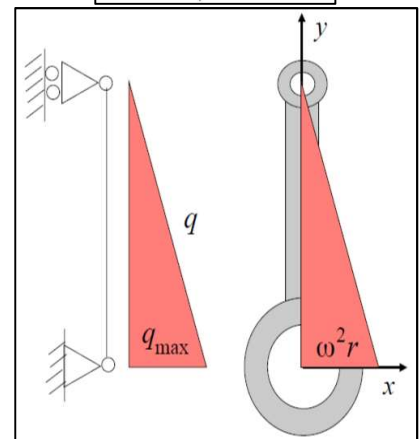
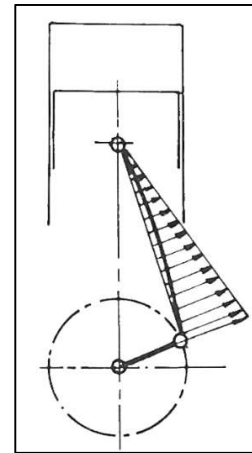


Figure 2-6 Bending Load

## 2.6 Composite Connecting Rod

The previous calculations can be now applied for the new geometry and material, to evaluate benefits and disadvantages.

Due to the geometry change, also the centre of gravity has changed its position.

<b>Small Eye to G Distance</b>	$x_1 = 96,08\text{mm}$
<b>Big Eye to G Distance</b>	$x_2 = 33,29\text{mm}$

Table 2-3 G Distance

For the mass:

<b>Connecting Rod Mass</b>	$m_{cr} = 201,98\text{g}$
<b>Small eye mass</b>	$m_{cr,a} = 51,97\text{ g}$
<b>Big eye mass</b>	$m_{cr,r} = 150,00\text{ g}$

Table 2-4 Rod Masses

Before going ahead in the discussion, it is important to remind that also the pin has been modified using composite material.

<b>Steel Pin</b>	$m_{wp} = 72\text{ g}$
<b>Composite Pin</b>	$m_{wp} = 23,91\text{ g}$

Table 2-5 Wrist Pin Masses

### **3 HyperMesh Analysis**

The FEM analysis was conducted using Altair HyperMesh for the mesh optimization and Optistruct as solver. The main problem using this software was the not complete implementation of the composite card material for 3D element.

A fundamental characteristic of the carbon fibre is the orientation of the fibres: acting on these directions, the mechanical behaviour changes dramatically.

At the state of art of the software, the management of these directions is not simple, especially because the material orientation tool doesn't show the fibres direction.

So, the direction of the fibres was supposed accordingly with the definition expressed in the next paragraph, which has been found on the Altair information material.

#### **3.1 Property Card**

##### **3.1.1 PSOLID**

Considering that condition, it was proceeded step by step, starting from simplified model and checking that it converges each time a modification was done.

Concerning the Property Card setup, it is started from PSOLID, which is the most known. PSOLID allows to use the Material Card MAT9ORT for orthotropic material, but it is not designed for composite material.

So, the 3D mesh was organized in components: each component represented a set of layers of carbon fibres. In first analysis, it was assumed that each carbon layer had 0.2mm as thickness and each mesh component contained 5 layers of carbon fibre.

With that procedure, should be possible to assign to each component different material or same material but with different orthotropic characteristics.

Obviously, it is a ploy to circumvent the non-suitability of PSOLID for the composite material.

Unfortunately, the material orientation tool seems to have some problem in managing the change in material orientation. It wasn't possible to understand why.

For the two pins, the Card was PSOLID, too. In this case, nothing strange because they are in steel, so MAT1 as isotropic material characteristic has been chosen.

### 3.1.2 PCOMPLS

To increase the precision of the results, a new property card was developed. PCOMPLS is a new property card that Altair has developed specifically for composite material.

The software is optimized for laminate elements (2D shells). The optimization of all the functions for 3D elements is still in process.

In particular, in the property card wasn't available the choice of the angle of the fibre direction and the material orientation tool doesn't show the material orientation.

The solution for this lack would be to export the .fem file, to open it with the Text Editor and to modify the elements in the grid related to the above-mentioned angle. Then, importing the file .fem again in HyperMesh, the angle box in the property card would result editable. It remains the problem related to the possibility to show the fibre orientation.

As consequence, the setup of the angle value should be based on the definition of the angle itself, given in the Altair University tutorial\*.

It's important to remember that this property defines global ply-based composite properties for layered solid shell composites. PCOMPLS entry is only supported for CHEXA and CPENTA elements (so it's important to delete all 2D meshes), linear and nonlinear analysis (small and large displacement and contacts) and MAT1, MAT9 and MAT9ORT material types.

Below, the format of PCOMPLS Card is reported, even if, due to its limitations, it was chosen to not continue this path.

(1)	(2)	(3)	(4)	(5)
PCOMPLS	PID		CORDM	
	C8		INT8	
	ID1	MID1	T1	THETA1
	ID2	MID2	T2	THETA2

Table 3-1 PCOMPLS Format

In which:

PID	Unique composite property identification number
CORDM	Identification number of the material coordinate system
IDi	Global Ply ID
MIDi	Material ID for the ply defined via the previous IDi field
Ti	Defines the actual thickness of the ply specified via the IDi field
*THETAi	Orientation angle of the ply within the ply plane*. The X-axis coordinate system defined via CORDM (basic system, if blank) is projected onto the ply plane. The orientation angle is measured from this projected X-axis along the projected Z-axis (Comment 4).

Table 3-2 PCOMPLS Details

\*The ply plane is defined perpendicular to the thickness direction of the composite element. The orientation angle is measured positive counter clockwise direction from the projected X-axis about the local Z-axis of the ply.

The actual ply thicknesses depend on the actual total geometric thickness of the solid element.

The calculation is as follows:

$$T_{actual}^{ply_i} = T_{actual}^e \left( \frac{T_i}{T_1 + T_2 + \dots + T_N} \right)$$

Equation 3-1 Ply Thickness Evaluation

$T_{actual}^{ply_i}$  is the actual thickness of the ply “i”

$T_{actual}^e$  is the actual (or geometric) thickness of the composite element

$T_i$  is the user-defined ply thickness via the  $T_i$  fields on the PCOMPLS entry

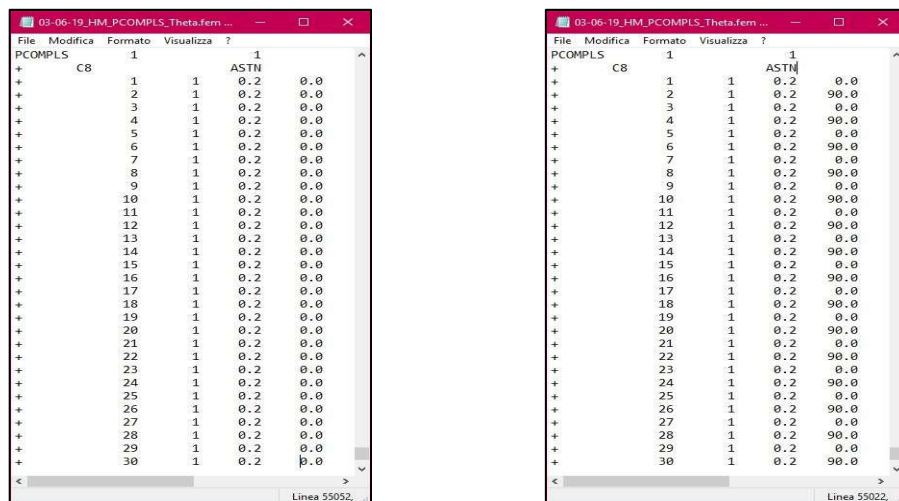


Figure 3-1 Text Editor for PCOMPLS

### 3.2 Models

The aim of this project is to design a new geometry respecting these principal constraints:

- geometry suitable with the production process of the carbon fibre material
- lighter than actual connecting rods
- better distribution of the stress caused by the assembly preload, through the material

For the first two requirements, it should be enough to maintain a classical shape, using threaded inserts in the carbon fibre rod. This would save about the 50% in weight with respect to the steel rod.

An example in the figure:

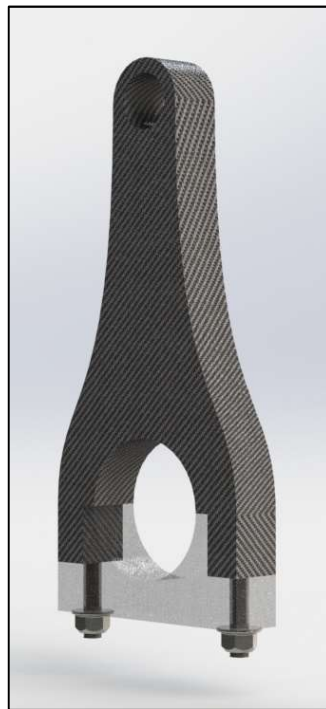


*Figure 3-2 Connecting Rod with Threaded Inserts*

But to have a better stress distribution, it was necessary to design a new way to mount the cap on the stem, giving at the same time the enough preload force to avoid the opening of the cap during the working cycle.

First, it should be considered that the production process consists in doing a stack of sheets of carbon fibre. The sheets should be pre-cut with the shape of the rod on the plane perpendicular of the crankshaft axis.

### 3.2.1 Transversal Holes Model

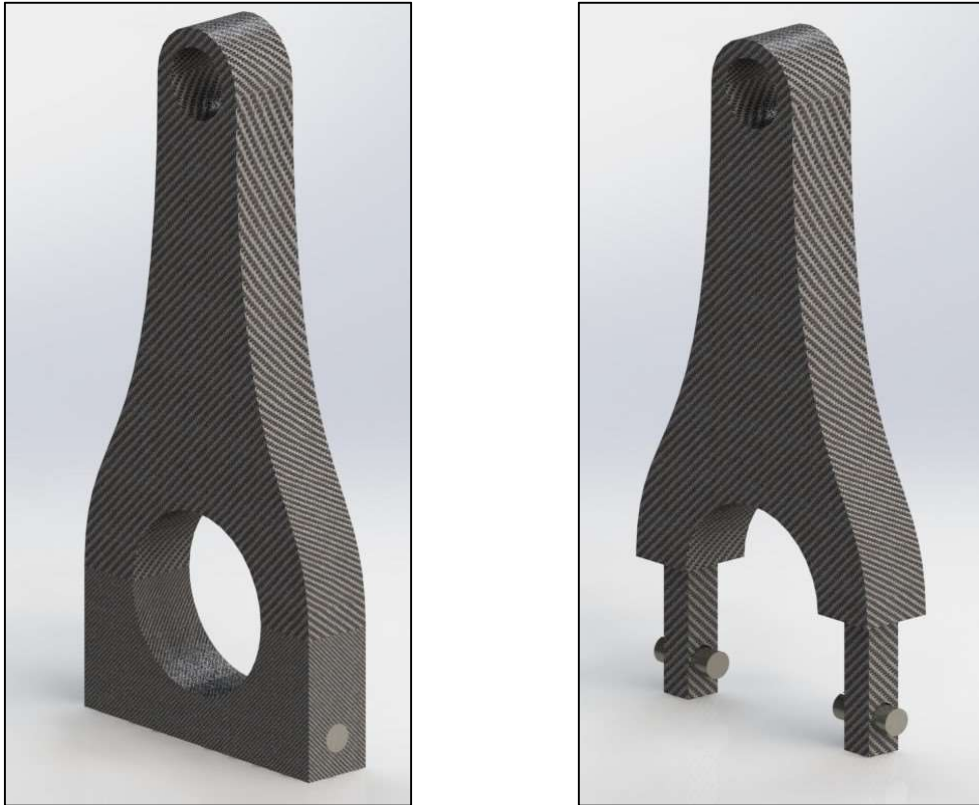


Figure 3-3 Transversal Holes Model

In this first version, two steel pins were used to join the cap with the stem. The holes in the cap had a misalignment of some tenth of millimetres with respect to the holes on the legs of the stem: in that way, the preload was given.

The optimization of the geometry was argument of the thesis of Ömer Faruk Kale, according to these parameters:

1. Height of profile (12mm to 15mm)
2. Width of profile (8mm to 12mm)
3. Location of holes and pin (will be translated 3mm)
4. Radius of holes and pin (2.5mm to 4.5mm)
5. Misalignment between holes (starting from 0.2mm)

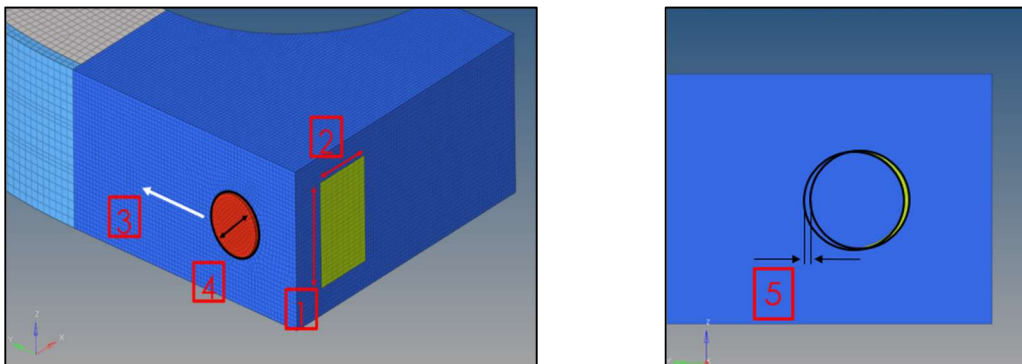


Figure 3-4 Optimization Parameters



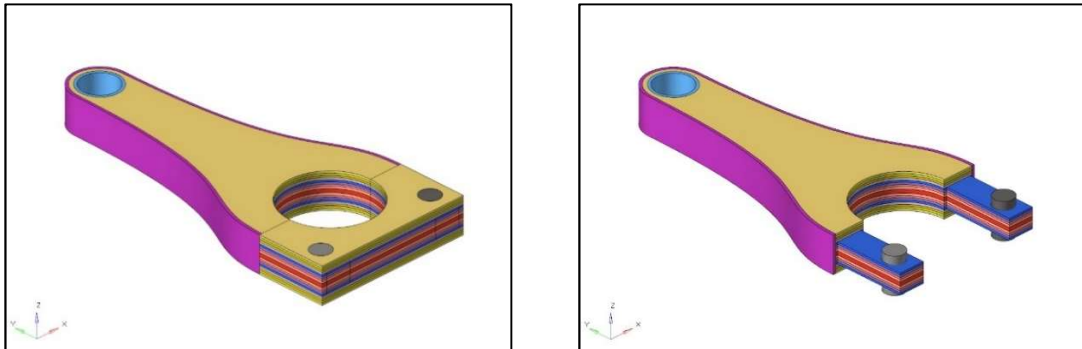


Figure 3-7 Layered Model

As it can be seen in the previous pictures, the rod was meshed into layers. Each layer was considered as a single component. The reason for this choice has been explained in the Property Card, PSOLID paragraph.

The external layer, purple in the mesh, represents a sort of peel to coat the edge of the carbon fibre sheets.

The layer in the small eye, sky blue in the mesh, represents the circumferential layer of carbon fibre, to better support the load transferred by the pin to the rod.

Unfortunately, due to the impossibility to choose the material orientation, as said before, these layers weren't simulated: they are a suggestion for a future development.

So, the model analysed doesn't present a division into components:

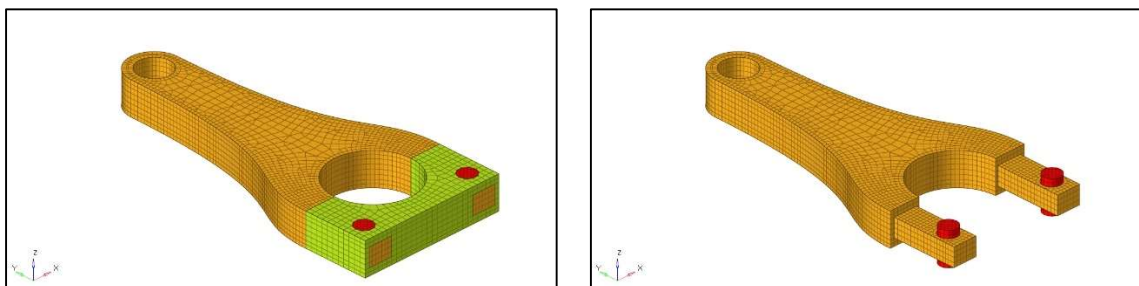


Figure 3-8 Model Mesh

Here the material organization: blue is carbon fibre, red is steel.

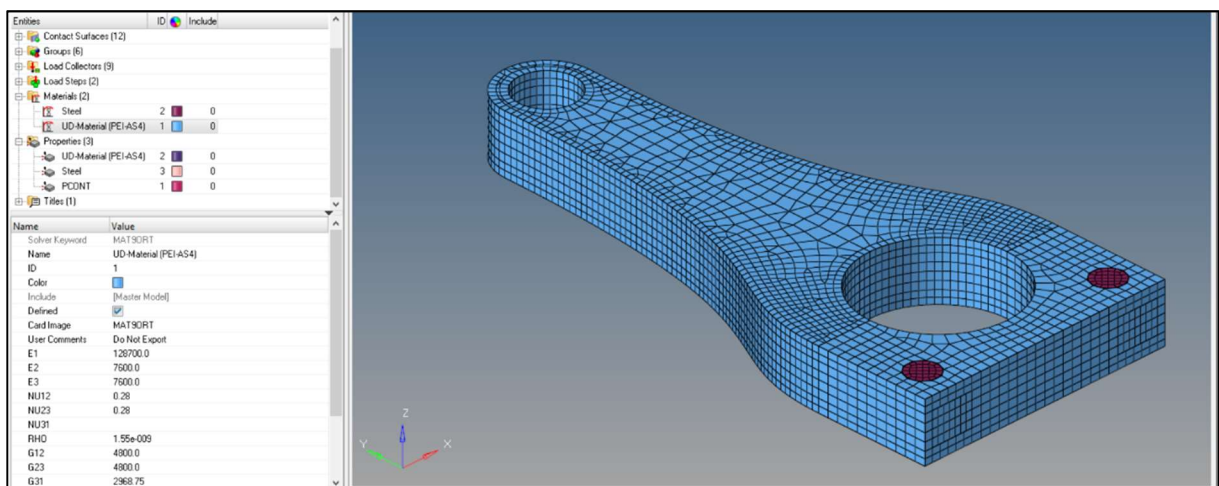
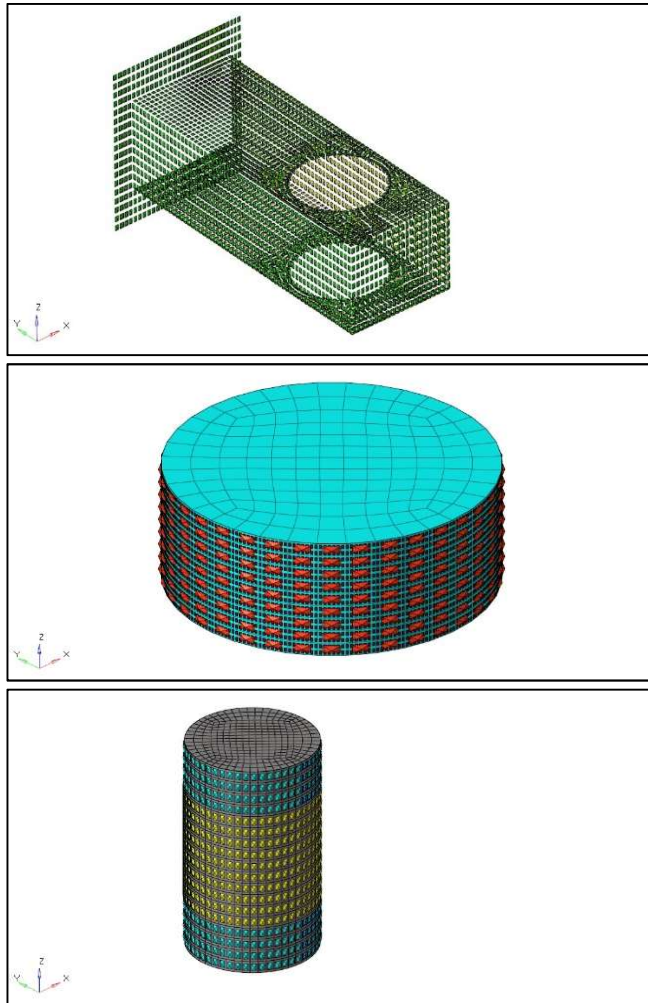


Figure 3-9 Material Organization

Concerning the contact surfaces, they have been defined using the Property Card PCONT, which allows to set the friction coefficient: in this case the value 0.2 was chosen.

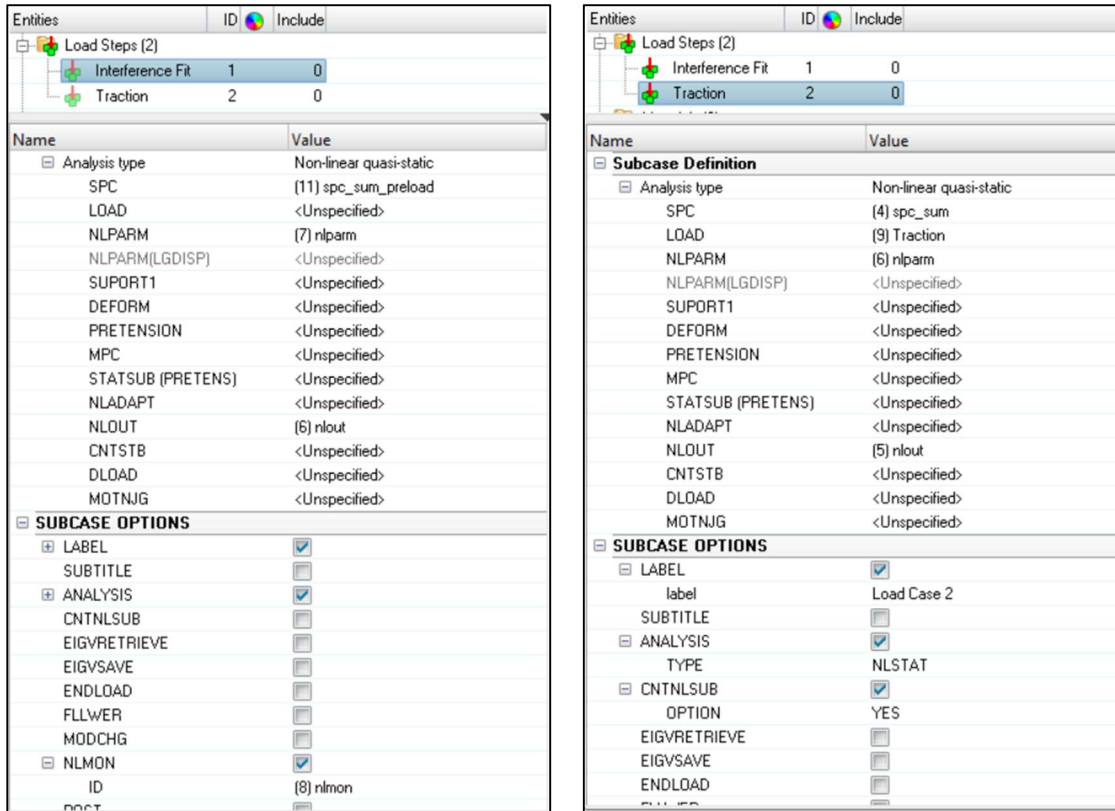
The contact surfaces were:



Between the legs of the rod and the cap: they can slide
Between the crankshaft, the stem of the rod and the cap: they can slide
Between the cap, the pin and the leg of the rod: there must be interference fit enough to hold the rod close around the crankshaft

Figure 3-10 Contact Surfaces

The load steps were two: the first simulates the interference fit between the pins and the two parts of the rod, the second one simulates the load that we want to check (traction, bending, compression). This method is used to simulate the stress due to the preload which should avoid the rod to open during the working cycle.



<p><b>Interference Load Step:</b>                  note that in Analysis, Type, NLSTAT was selected.</p>	<p><b>Traction Load Step:</b>                  note that the checkbox CNTNLSUB allows to Optistruct to continue the simulation of the Subcase 2 from the last load step of the subcase 1.</p>
--	---

Figure 3-11 Loadsteps

The load collectors NLPARM, NLOUT, NLMON help the solver to converge easily, setting up the number incremental steps and the number of iterations.

The setup of the constrains and of the loads will be explained in the results paragraph.

### 3.3 Failure Criterion

Failure Index  $F$  is the only way to compare different solutions since it combines stress on different directions. As composite materials are the subject of this project, a common failure index would fail. So, an appropriate failure criterion must be chosen.

#### 3.3.1 Tsai-Wu criterion

This criterion was originally proposed for anisotropic materials. Subsequently the model was spread for orthotropic materials. The Tsai-Wu criterion is expressed through a quadratic polynomial expression of stresses with tensorial coefficients. The tensorial expressions allows a general applicability of the criterion to describe materials.

The most common form of the criterion employs the following failure function for orthotropic materials and its expressed in their principal axes:

$$F = F_{11}\sigma_1^2 + F_{22}\sigma_2^2 + F_{33}\sigma_3^2 + 2F_{23}\sigma_2\sigma_3 + 2F_{13}\sigma_1\sigma_3 + 2F_{12}\sigma_1\sigma_2 + F_1\sigma_1 + F_2\sigma_2 + F_3\sigma_3 + F_{44}\tau_{23}^2 + F_{55}\tau_{13}^2 + F_{66}\tau_{12}^2$$

*Equation 3-2 Tsai-Wu Formula*

To deliver a failure criterion, it is claimed that the material is safe if  $F < 1$ , while the critical condition starts when  $F = 1$ .

It is generally unsatisfactory to consider laminated composites as an orthotropic material as far as their strength predictions are concerned, even if they exhibit orthotropic elastic behaviour macroscopically. Unlike elastic properties which are dominated by the global behaviour at a macroscale, strengths are governed by localized features at a micro level. Even in so-called non-local theories, it is still a local problem with a focus on a small neighbourhood of the point of singularity.

Given a random distribution of fibres in the cross-section of an UD (Unidirectional) composite component, transverse isotropy is sufficiently satisfactory to describe the behaviour of the UD composite, for which one has:

$F_{33} = F_{22};$	$F_{13} = F_{12};$	$F_3 = F_2;$	$F_{55} = F_{66};$	$F_{23} = F_{22} - 0.5F_{44}$
--------------------	--------------------	--------------	--------------------	-------------------------------

In this case the Tsai-Wu failure function can be reduced to:

$$F = F_{11}\sigma_1^2 + F_{22}(\sigma_2^2 + \sigma_3^2) + (2F_{22} - F_{44})\sigma_2\sigma_3 + 2F_{12}\sigma_1(\sigma_3 + \sigma_2) + F_1(\sigma_1 + \sigma_2) + F_2\sigma_3 + F_{44}\tau_{23}^2 + F_{66}(\tau_{13}^2 + \tau_{12}^2)$$

*Equation 3-3 Tsai-Wu Reduced*

where the coefficients can be determined from the conventional strengths of UD composites as

$$F_{11} = \frac{1}{\sigma_{1t}^* \sigma_{1c}^*}; F_{22} = \frac{1}{\sigma_{2t}^* \sigma_{2c}^*};$$

$$F_1 = \frac{1}{\sigma_{1t}^*} - \frac{1}{\sigma_{1c}^*}; F_2 = \frac{1}{\sigma_{2t}^*} - \frac{1}{\sigma_{2c}^*};$$

$$F_{44} = \frac{1}{(\tau_{23}^*)^2}; F_{66} = \frac{1}{(\tau_{12}^*)^2}$$

*Equation 3-4 Tsai-Wu Coefficients*

with  $\sigma_{1t}^*$  and  $\sigma_{1c}^*$  being the tensile and compressive strengths of the material along fibres,  $\sigma_{2t}^*$  and  $\sigma_{2c}^*$  those in the direction transverse to the fibres, and  $\tau_{12}^*$  and  $\tau_{23}^*$  the shear strengths along and transverse to fibres. These strengths properties were supplied by the producer of the material.

Anyway, the coefficient  $F_{12}$  has not yet been specified and should be ideally determined through biaxial stress tests. Given the difficulties in conducting this type of tests, no standard method is available to determine it.

According with Tsai and Wu, the failure criterion gives rise to a closed ellipsoid. This condition can be employed to evaluate  $F_{12}$  coefficient.

For most applications under in-plane stresses Equation 3-5 can be rewritten in its 2D form:

$$F = F_{11}\sigma_1^2 + 2F_{12}\sigma_1\sigma_2 + F_{22}\sigma_2^2 + F_{66}\tau_{12}^2 + F_1\sigma_1 + F_2\sigma_2$$

*Equation 3-5 2-D Tsai-Wu Formula*

As  $F_{12}$  is associated only with direct stresses  $\sigma_1$  and  $\sigma_2$ , some considerations can be made below when the material is subject to biaxial direct stresses. The critical condition can be simplified in this case to

$$F_{11}\sigma_1^2 + 2F_{12}\sigma_1\sigma_2 + F_{22}\sigma_2^2 + F_1\sigma_1 + F_2\sigma_2 = 1.$$

*Equation 3-6 F12 Coefficient*

This defines a typical conic section in the  $\sigma_1$ -  $\sigma_2$  plane. The condition for the failure locus in the  $\sigma_1$ -  $\sigma_2$  plane to be an ellipse is given largely as

$$F_{12}^2 < F_{11}F_{22}$$

*Equation 3-7 Failure Locus*

However, this only defines a range for  $F_{12}$ , which appears to be rather wide in most cases. The complete determination of  $F_{12}$  remains as an issue to be resolved. It has been left as an empirical parameter. One form of it has been suggested as

$$F_{12} = -\frac{1}{2}\sqrt{F_{11}F_{22}}$$

*Equation 3-8 Empirical F12*

which was expressed in terms of conventional strength properties. The justifications for the simplified form are:

- It falls in the range as defined by  $F_{12} = -\frac{1}{2}\sqrt{F_{11}F_{22}}$
- It allows itself to be degenerated to that of von Mises if the material is specialised to isotropic having equal tensile and compressive strengths.

The Equation 3-8 can be plotted, and it will be represented by an ellipse, as shown in Figure 3-12. The four conventional strength properties ( $\sigma_{1t}^*$ ,  $\sigma_{1c}^*$ ,  $\sigma_{2t}^*$  and  $\sigma_{2c}^*$ ) represents the intersecting point of the ellipse with the coordinate axis. These four points aren't enough to determine univocally an ellipse.

The interactive term  $F_{12}$  plays the role of providing another anchoring point so that the ellipse can be univocally determined. As it is possible to notice in Figure, different values of  $F_{12}$  tend to tilt the ellipse.

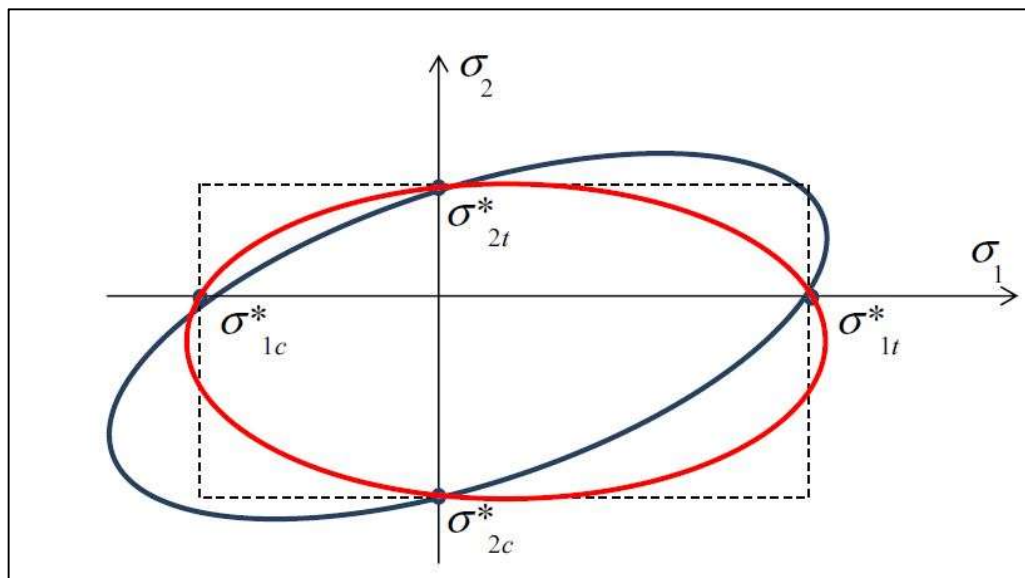


Figure 3-12 Tsai-Wu Ellipse

Unfortunately, the Tsai-Wu criterion has not still implemented for solid layered elements. The attempt using the Derived Function tool of HyperView has failed, because the result gave unrealistic values. Probably, it is since the PCOMPLS is not completely optimized for the solver Optistruct.

## 4 Conclusions

### 4.1 Mechanical Results

In conclusion, a first analysis of the benefits was done in terms of weight and forces, due to the utilization of the carbon fibre.

In terms of mass:

Component	Steel mass	Carbon fibre mass	Percentage variation
<b>Pin</b>	72g	23,91g	- 66%
<b>Connecting Rod</b>	428g	202g	-52%
<b>Total</b>	500g	225,91g	-55%
<b>Alternating Masses</b>	406,14g	293,88g	-28%
<b>Centrifugal Masses</b>	786,32g	624,46g	-20%

Table 4-1 Mechanical Results

For the alternating force, we should consider that it changes according to the angle of the crank shaft, for a fixed angular speed.

The values of the forces are showed in Figure 3, noting that the x-axis is downward. This means that in traction phase, the force values are negative since their direction is opposed to x-axis (Figure II-2); vice versa in compression phase.

The most stressed condition due to the inertia is at the end of the exhaust phase, when the piston is at the top dead centre (TDC). It corresponds to a traction condition for the rod, while at the end of the expansion phase the rod undergoes to a compression stress.

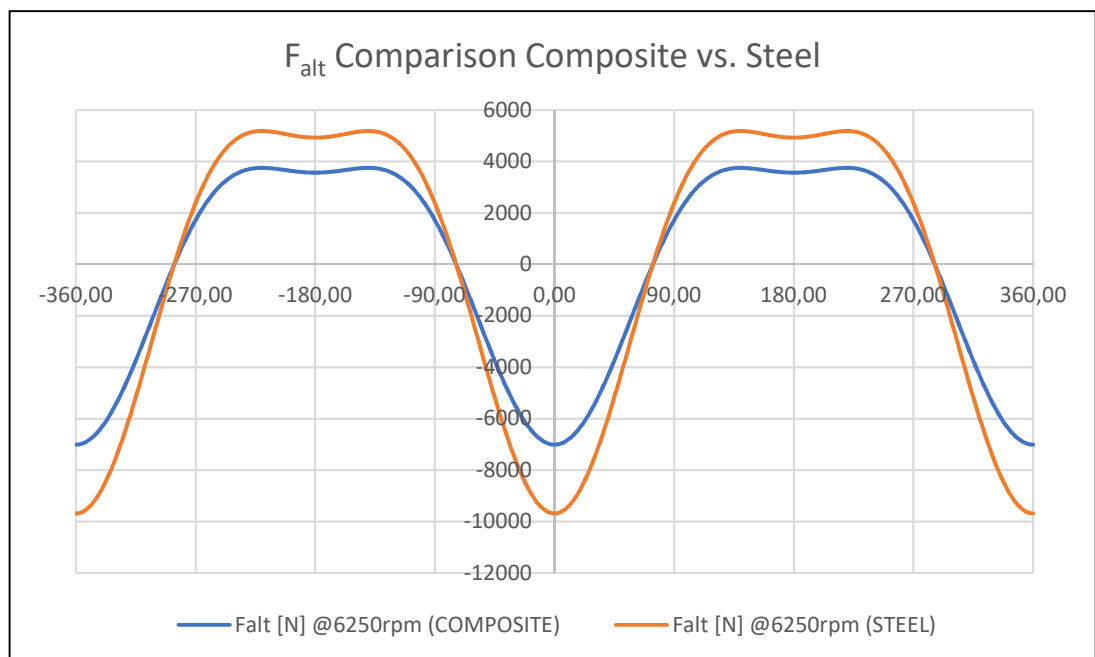


Figure 4-1 Alternating Force: Steel vs Composite

In terms of maximum values:

	Steel	Composite	Percentage Reduction
<b>Traction Force TDC</b>	-9687 N	-7096 N	-27,6%
<b>Compression Force BDC</b>	5184 N	3751 N	-27,6%

Table 4-2 Max Force Values

For the centrifugal force  $F_{\omega}$ , the values are:

Steel	Composite	Reduction
14147 N	11235 N	-20,6%

Table 4-3 Centrifugal Force Values

The equation for the torque acting on the single crank mechanism is equal to:

$$T = Fr \left( \sin\theta + \frac{\lambda}{2} \sin 2\theta \right)$$

Equation 4-1 Single Crank Mechanism Torque

Where F is the resultant force acting on the crank mechanism, equal to the sum of the force due to the gas pressure  $F_g$  and the alternating force  $F_a$ :

$$\begin{cases} F = F_g + F_a \\ F_g = [p_g(\vartheta) - p_0] \frac{\pi D^2}{4} \\ F_a = -m_a \omega^2 (\cos(\vartheta) + \lambda \cos 2\vartheta) \end{cases}$$

Equation 4-2 Resultant Force on Crank Mechanism

The gas pressure force considers the gas pressure inside the combustion chamber at each crank degree  $p_g(\vartheta)$  and the pressure in the crankcase  $p_0$ , equal to the environment pressure if the crankcase would be open.

The torque result is showed in the following plot:

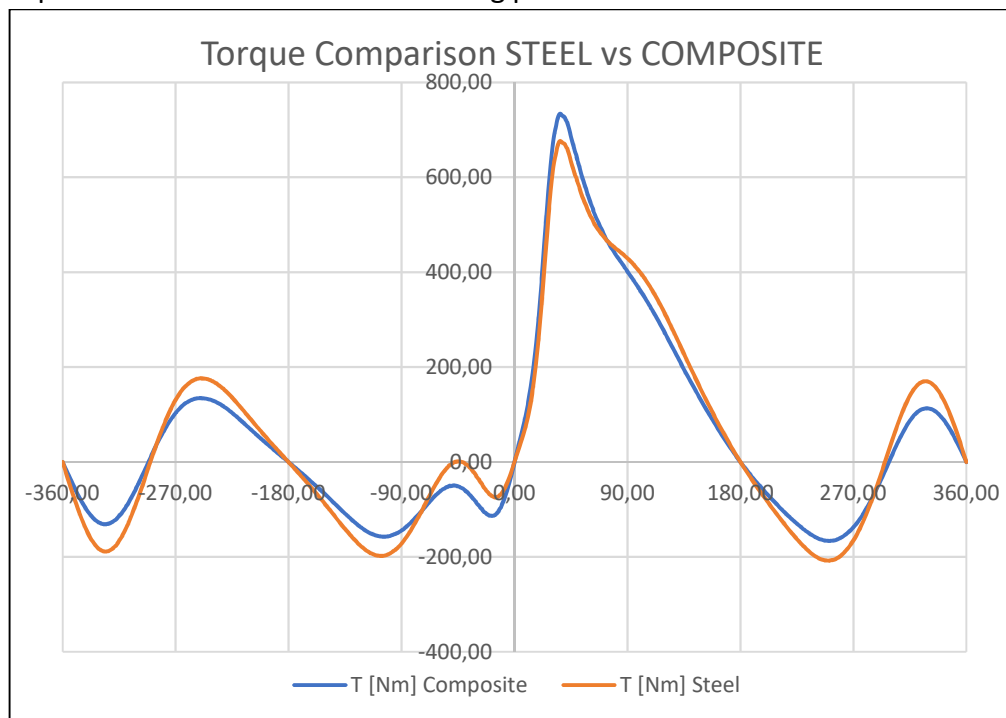


Figure 4-2 Torque Comparison

As it is possible to see in, the torque acting on a single crank mechanism changes significantly: the torque with composite material components has a higher peak value due to the lower inertial force. Indeed, the inertial force effect is opposite to the gas pressure effect. The reduction of the inertial force plays a beneficial role in the generation of the torque, increasing its value during the combustion phase.

It is also possible to notice that the oscillation around the x-axis are lower in the case of the composite components with respect to the steel components. This is still linked to the lower inertial force.

From the engine block point of view, the forces on the block can be summarized in the following way:

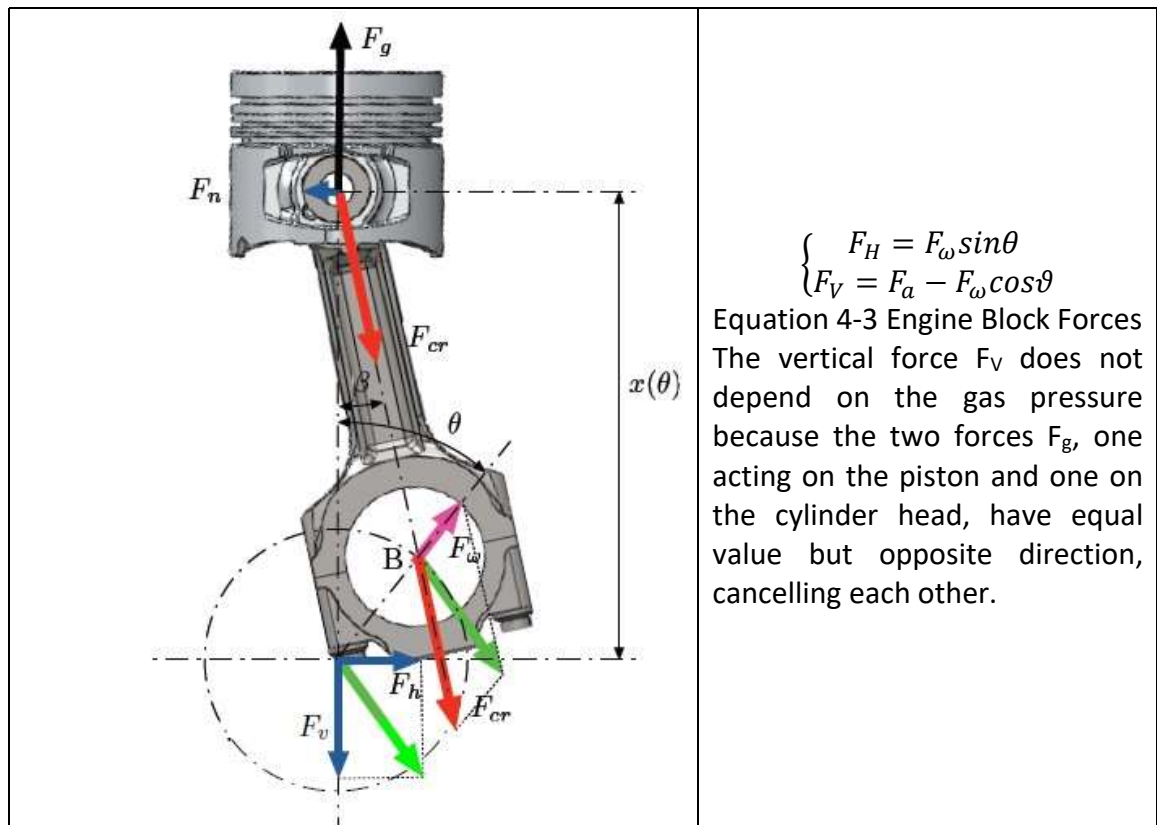


Figure 4-3 Engine Block Forces

The introduction of composite components would lead to a considerable reduction of these forces on the engine block. Referring to the maximum values<sup>(\*)</sup> of  $F_V$  and  $F_H$ :

Steel		Composite		Reduction
$F_{H, Steel}$	14147 N	$F_{H, Composite}$	11235 N	20,58 %
$F_{V, Steel}$	19074 N	$F_{V, Composite}$	14800 N	22,41 %
$F_{Total, Steel}$	23748 N	$F_{Total, Composite}$	18581 N	21,76 %

Table 4-4 Force Reductions

(\*) since only the maximum values was used for the comparison, the reduction percentage should be seen as the maximum percentage of force reduction.

Summarizing, the consequences on the other engine parts should be:

- Smaller and lighter crankshaft, engine block and main bearings, due to reduced forces acting on them
- Smaller and lighter crankwebs and flywheel, due to the lower engine irregularity

## 4.2 FEM Results

In this paragraph the results of the different simulation are presented. The graphical results will show the stress distribution for each model.

Regarding the HyperView results, some clarifications should be done. The values showed in the results for the stress are in *MPa* and the strain in *mm*. To obtain *MPa* in HyperView, proper measure units must be selected. The density was set in *tons/mm<sup>3</sup>* in the Material card and the forces were set in *N*. The crankshaft and the pins were hidden to allow the correct visualization of the results.

The principal stress directions are analysed coherently to the following figure:

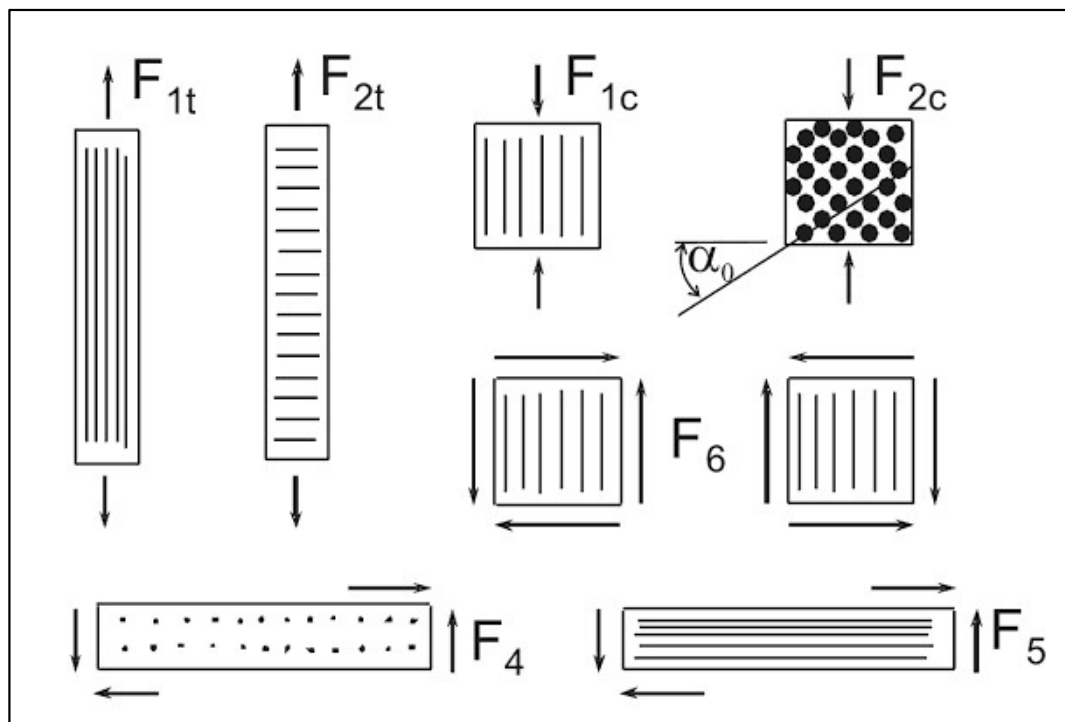


Figure 4-4 Principal Stress Directions

Where  $F_{1t}$  is the principal longitudinal stress and  $F_{2t}$  the principal transversal stress.

<b>Maximum longitudinal stress</b>	$F_{1t}$	2176 MPa
<b>Maximum transversal stress</b>	$F_{2t}$	46,7 MPa
<b>Maximum shear stress</b>	$F_6$	140 MPa

Table 4-5 Max Stress

#### 4.2.1 Tensile Load

First, it is shown the load that represents the traction: it is applied through RBE2 rigids, on the upper half-surface of the small eye. RBE3 should be more appropriate for load application. Nevertheless, it was chosen RBE2 because in the same point, it was applied also a constraint, which has to work with RBE2.

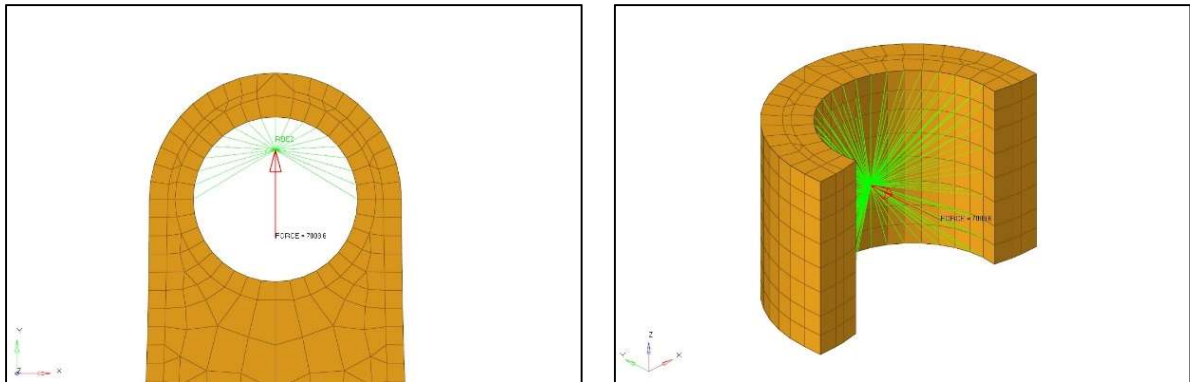


Figure 4-5 Traction Load

Then, it is shown the constraints.

For the preload step, the constraints avoid:

- Translation along x and z axis, on a lateral surface of the stem
- Every translation and rotation of the crankshaft, on both lateral surfaces

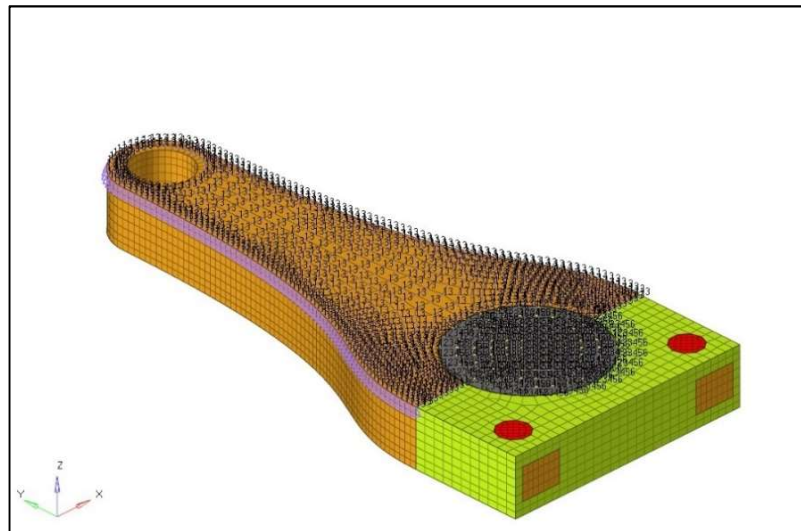


Figure 4-6 Preload Constraints

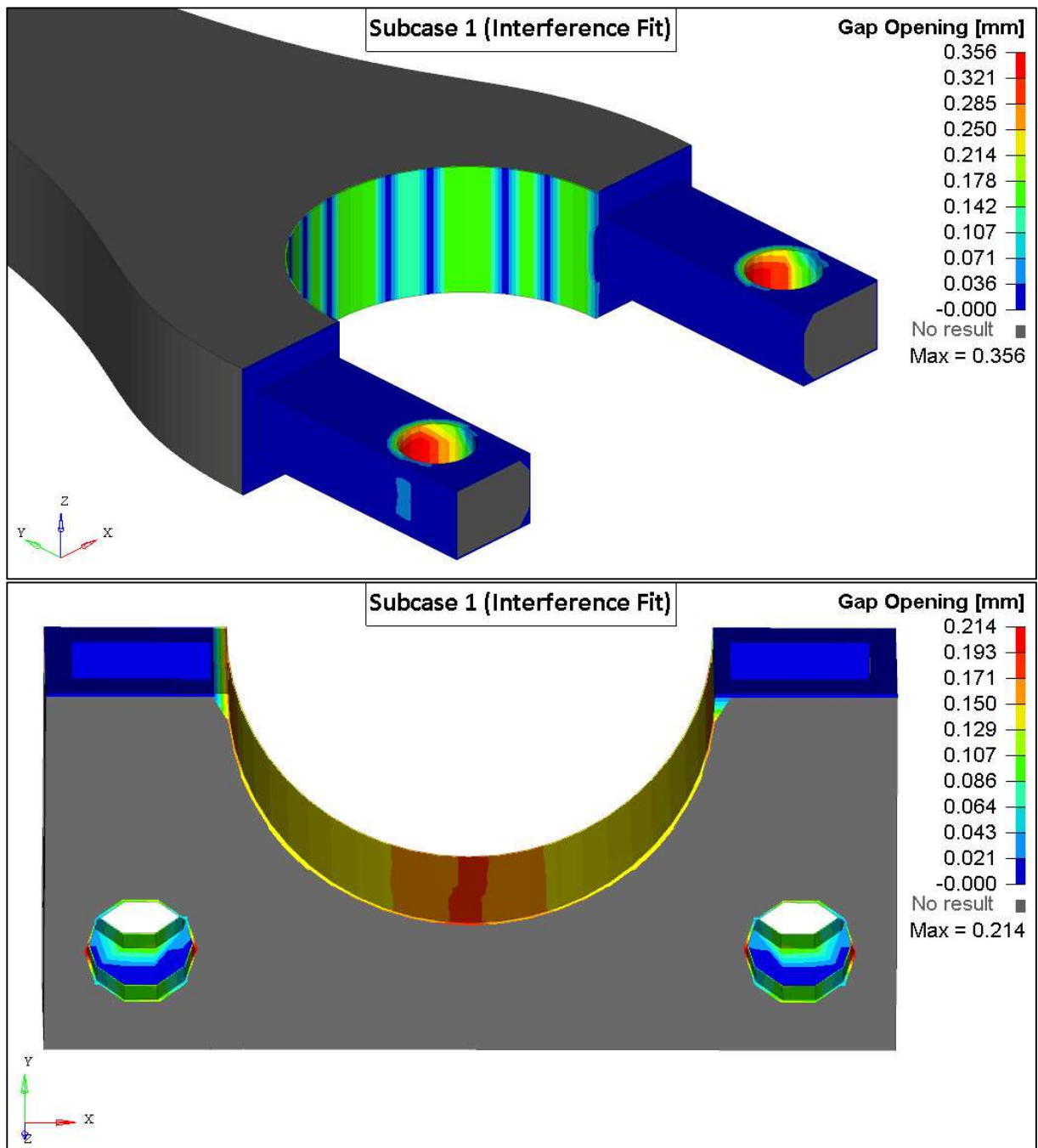


Figure 4-7 Preload: Gap Opening

As it can be seen, on the surfaces between the cap and the stem, there isn't gap opening, while the contact surfaces between the two parts of the rod and the crankshaft show few mm of gap opening. It isn't negligible.

The main aspect to be analysed in the future of this project should be the misalignment of the holes to provide the interference fit, avoiding deformations and gap openings.

In the next pictures, the contact status will be shown. The tiny asymmetry could be caused also by a not perfectly symmetric mesh.

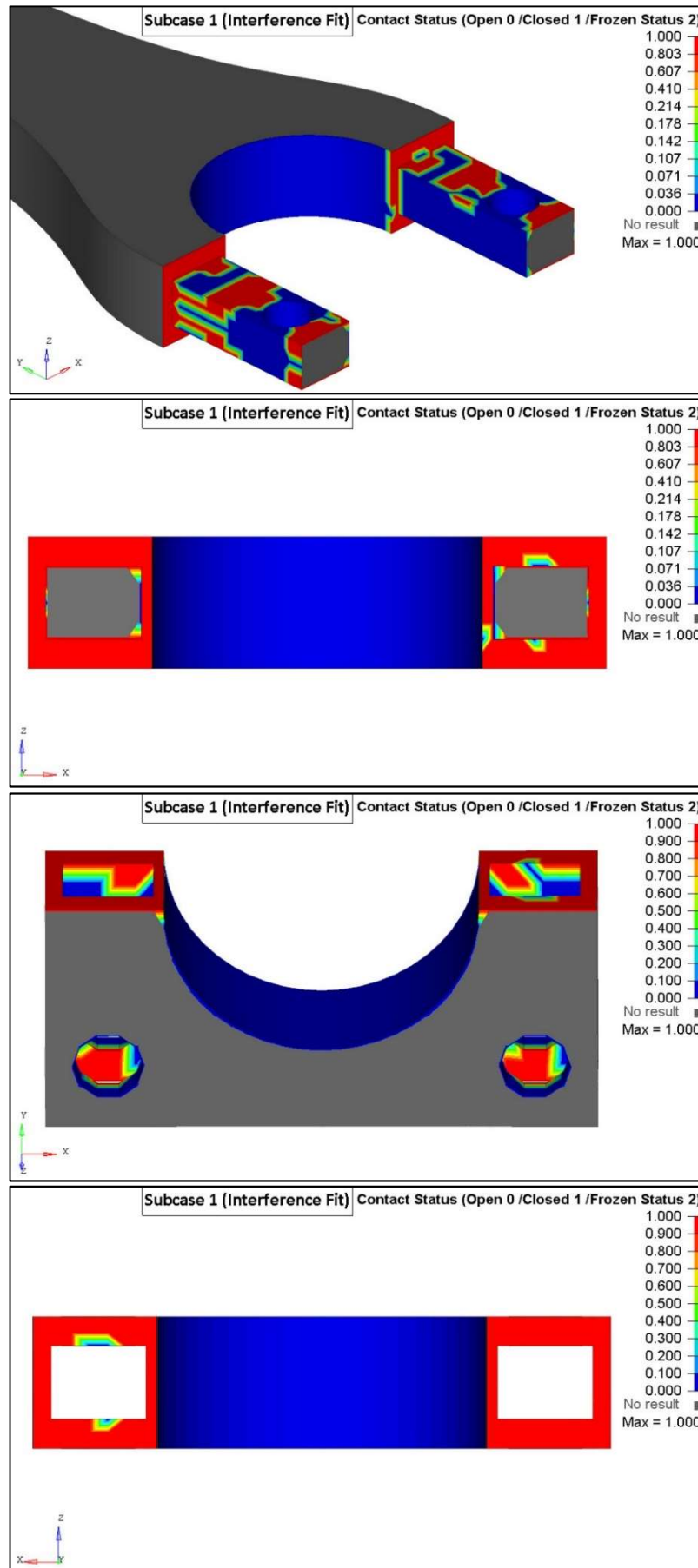


Figure 4-8 Preload: Contact Status

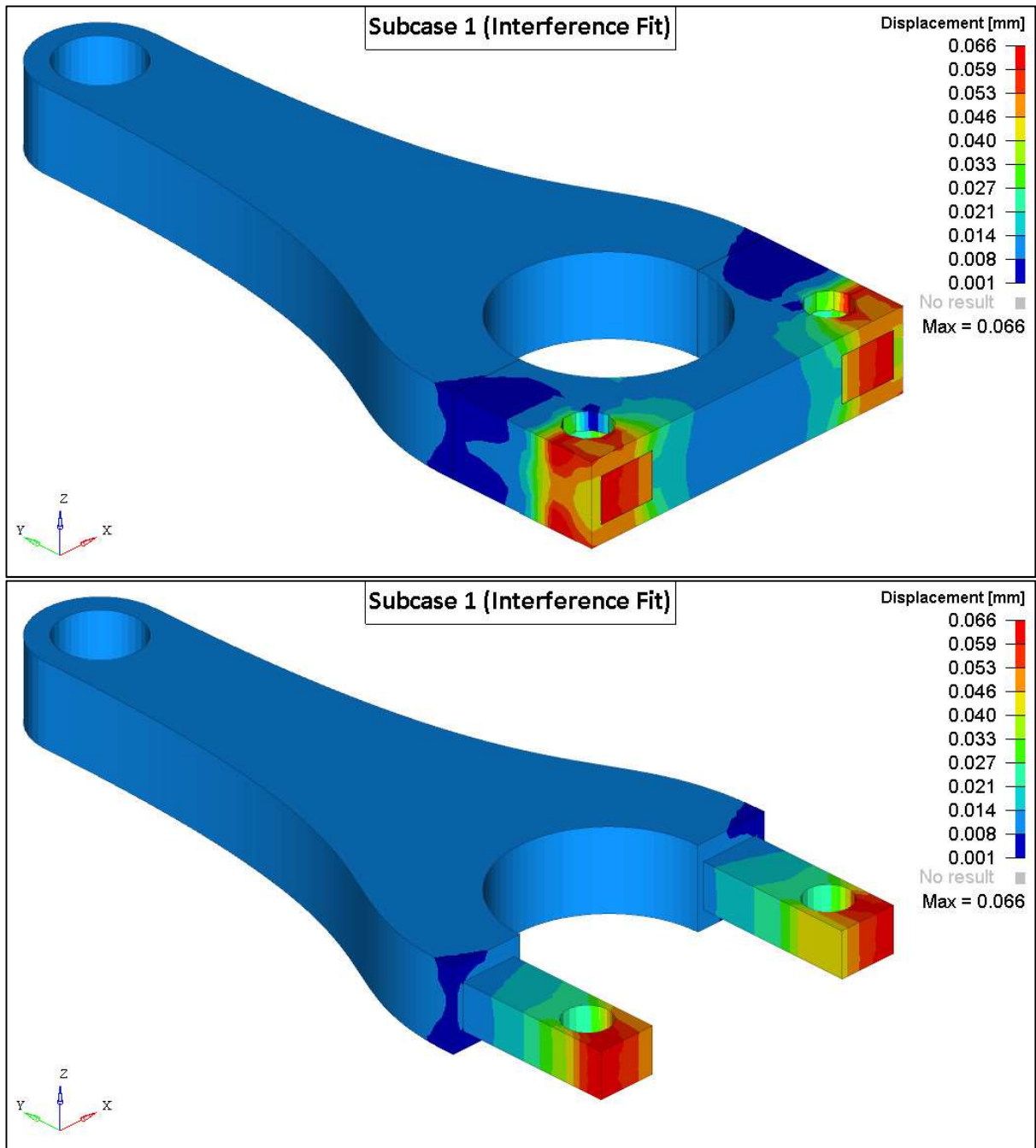


Figure 4-9 Preload: Displacement

As could be seen, the main deformation is the present in the pin holes zone.

These zones are the main stressed both in the preload step and in the main load steps. For this reason, the future development of this project must focus on the shape of these parts of the rod, modifying the dimensions of the pin holes, the layering of the carbon fibres and the dimensions of the legs of the rod.

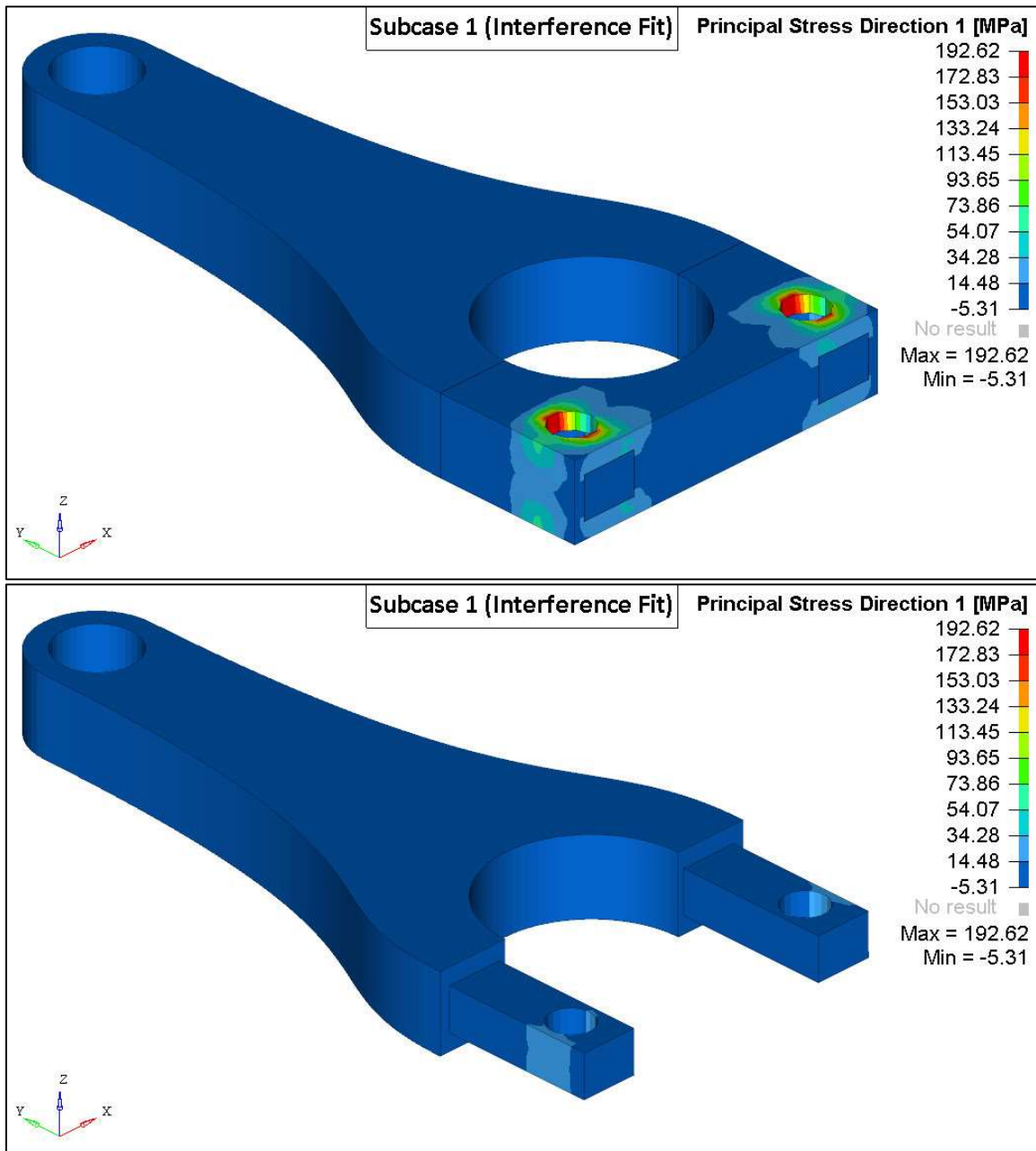


Figure 4-10 Preload: Principal Stress Direction 1

The Principal Stress Direction 1, P1 for simplicity, is the longitudinal direction. A Positive value means that the material is stretched. Again, the only interested region in the preload phase is around the pin holes.

Below, the P2 and P3 are represented. They are transversal stress directions, the values are both positive and negative: in the P2 they have similar absolute values, while in P3 the compression of the material is more significant than the stretching. It is an important aspect because our material doesn't behave in the same manner to the stretching and to the compression.

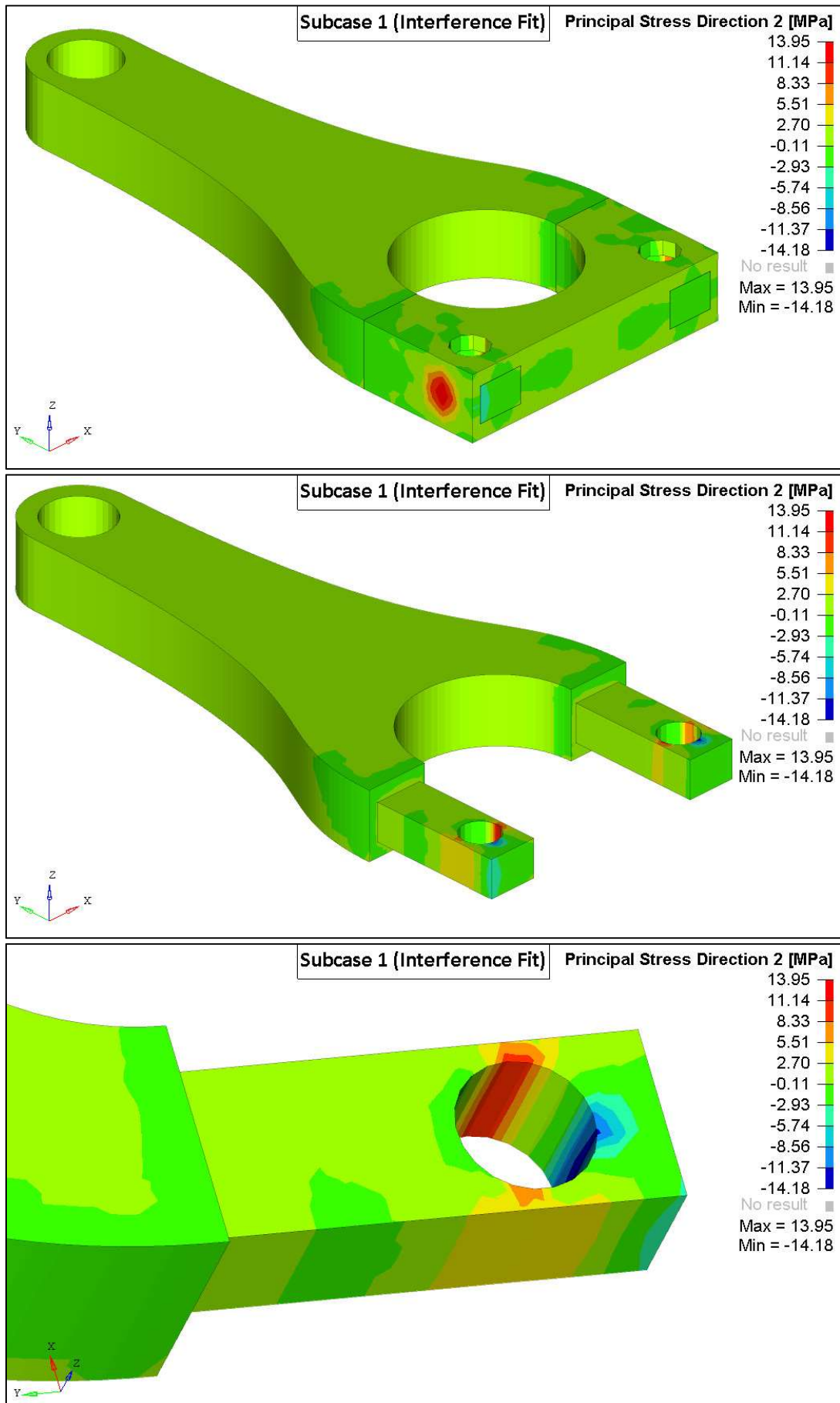


Figure 4-11 Preload: Principal Stress Direction 2

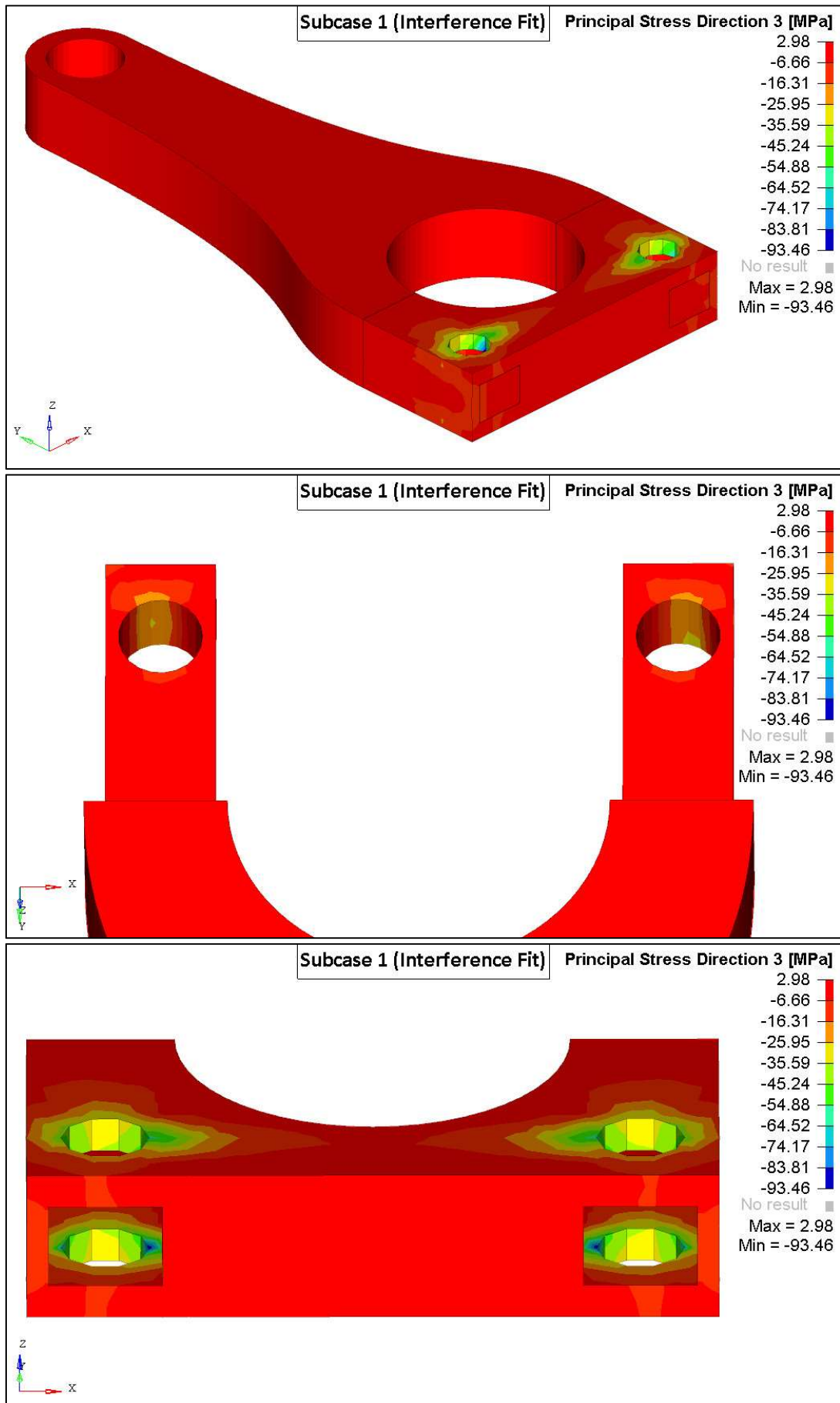


Figure 4-12 Preload: Principal Stress Direction 3

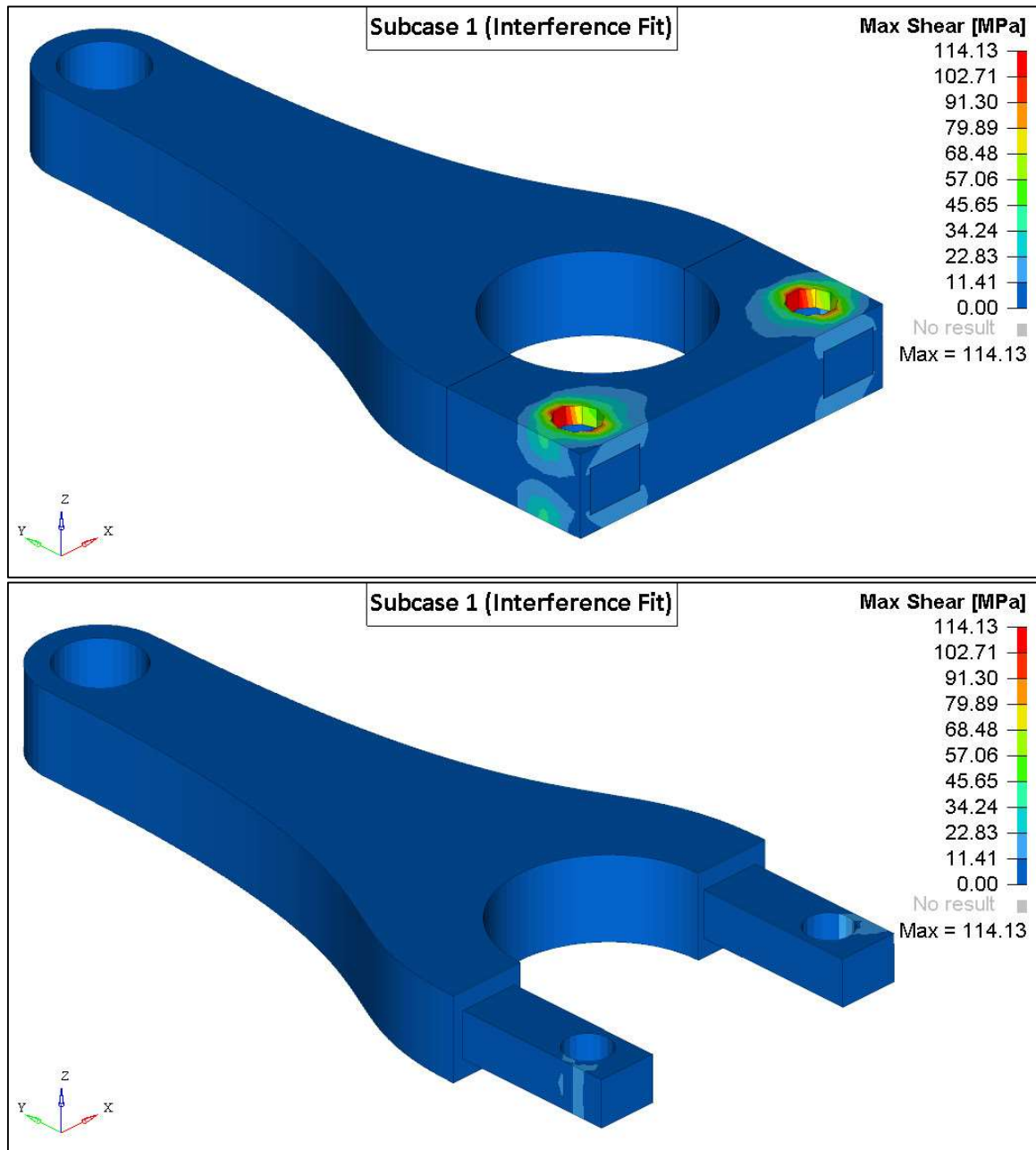


Figure 4-13 Preload: Max Shear

The shear around the pin holes suggest considering a different distribution of the material fibres or the usage of another composite with a better shear strength only in this zone.

For the traction load step, the constraints avoid:

- Translation along x and z axis of the nodes of the upper half-surface of the small eye
- Every translation and rotation of the crankshaft, on both lateral surfaces

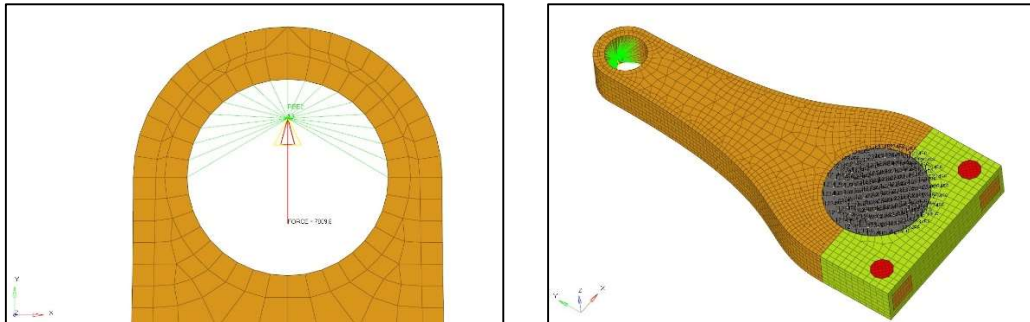


Figure 4-14 Traction Loadstep Constraints

The choice to have different constraints in the two step loads allows to get a more realistic stress result in the preload analysis.

It was observed a tiny rotation along z-axis, using in the preload simulation the constrain in the small eye, instead of the constraint on the entire lateral surface of the stem.

Below, the gap opening and the contact status show clearly that the 0.2mm of misalignment of the pin holes are not sufficient to guarantee the operation of the rod. In fact, as order of magnitude, a 0.01 mm opening is NOT acceptable since there would be oil leakage, while 0.001 mm is acceptable since it's below the machining tolerance.

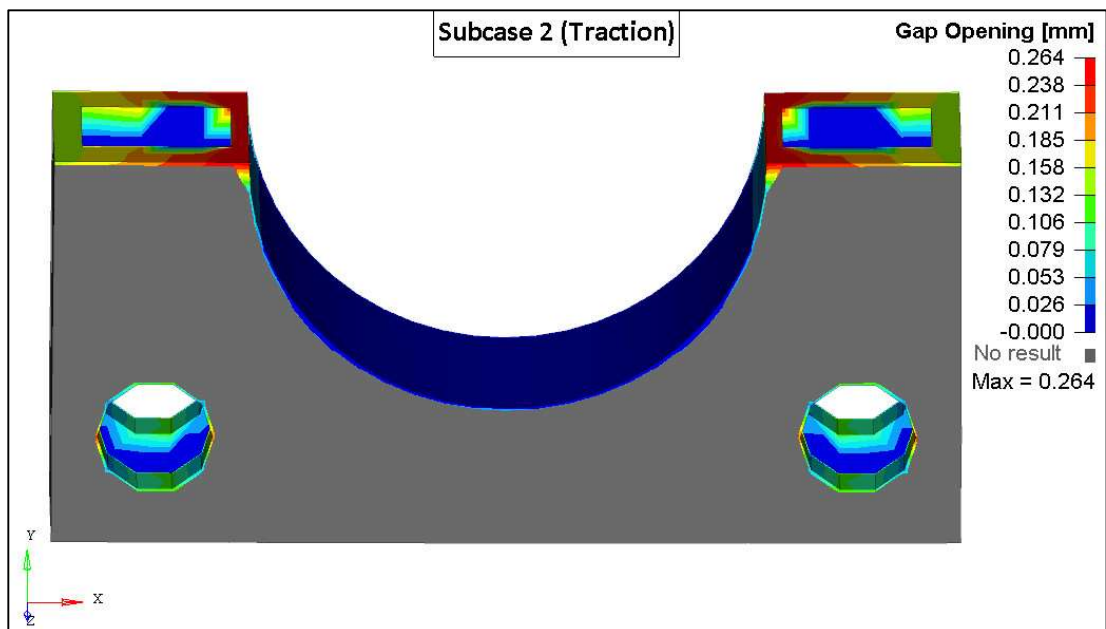
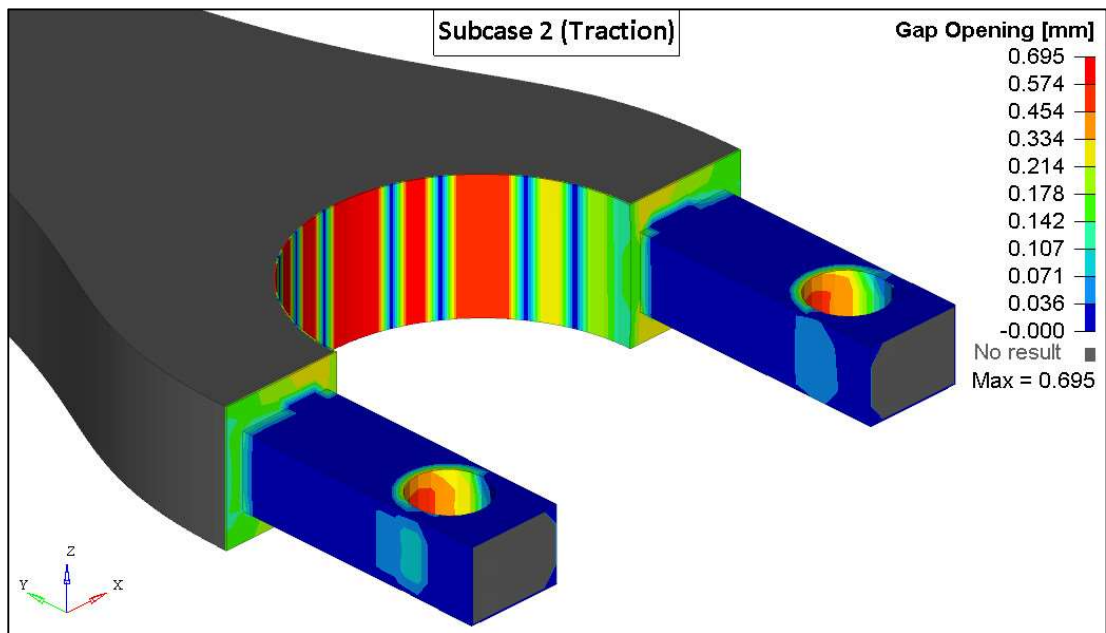


Figure 4-15 Traction: Gap Opening

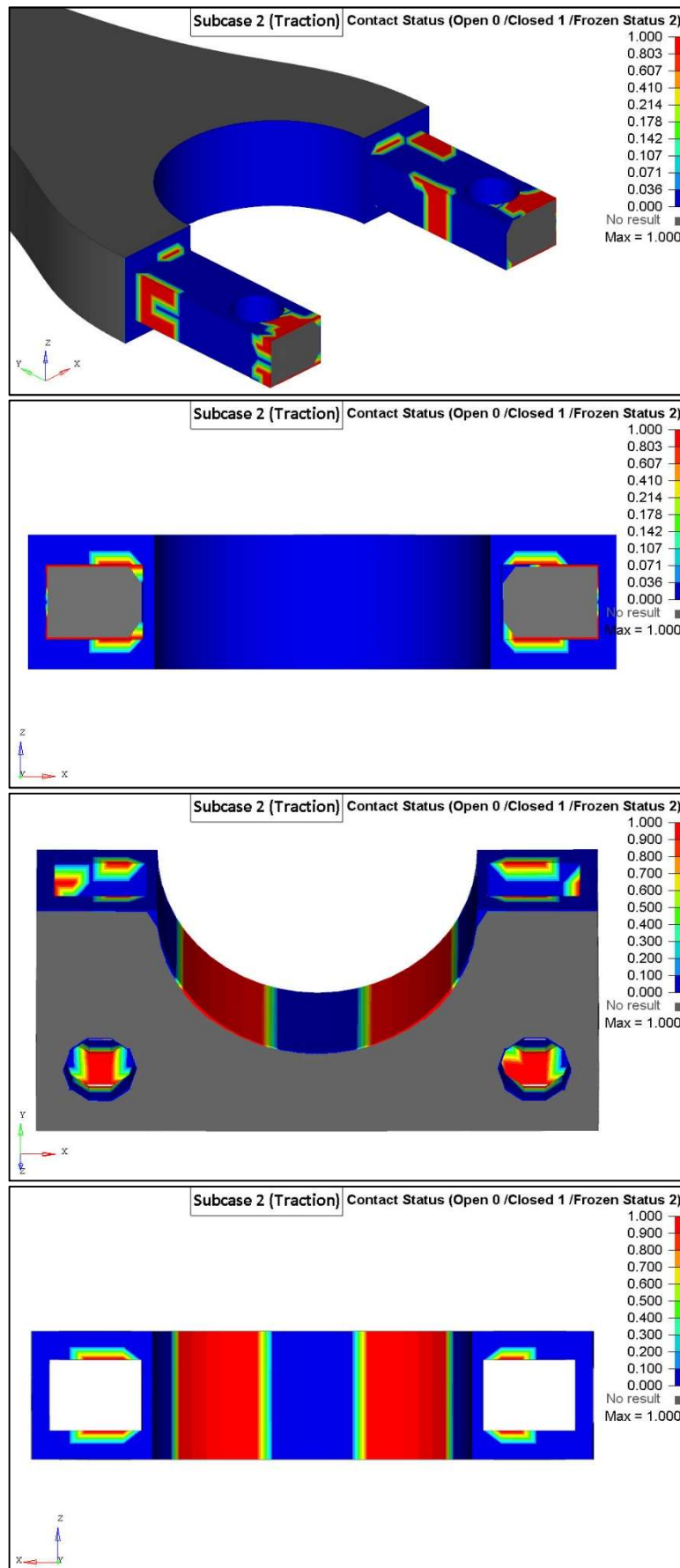


Figure 4-16 Traction: Contact Status

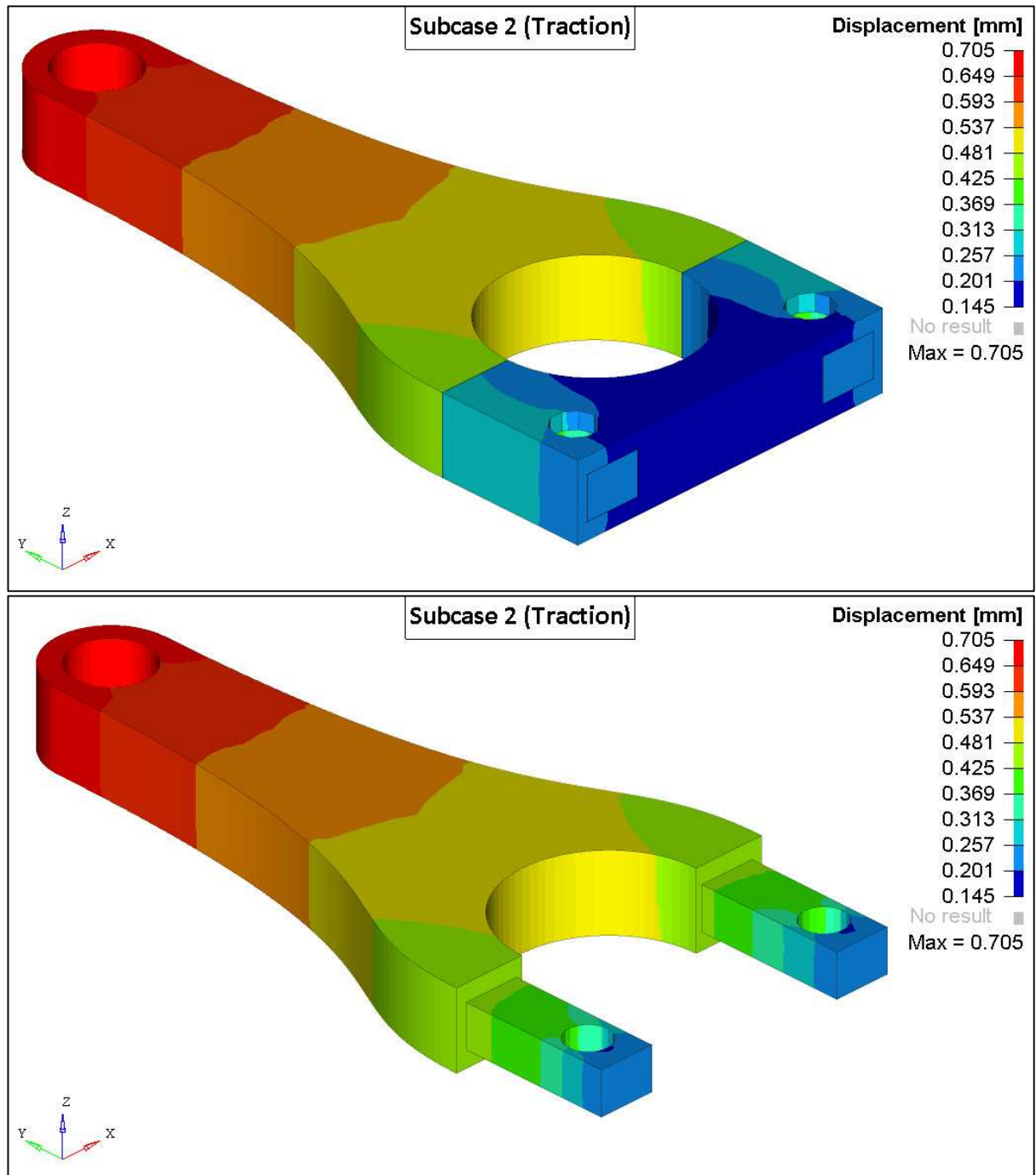


Figure 4-17 Traction: Deformation

Also, the deformation is too much evident. 0,7 mm is acceptable both for the working operations of the components and for the space available between the rod and the piston.

Below, it is shown the deformation enlarged as magnitude 20 times.

As it can be seen in the Table 4-5, for the P1 the stress the max values allowed is very high, while in the other directions P2 and P3, the limit values are lower than those calculated.

These considerations are not enough to say if the component will break or not: for this reason, a failure criterion must be adopted, to combine the stresses in the three directions.

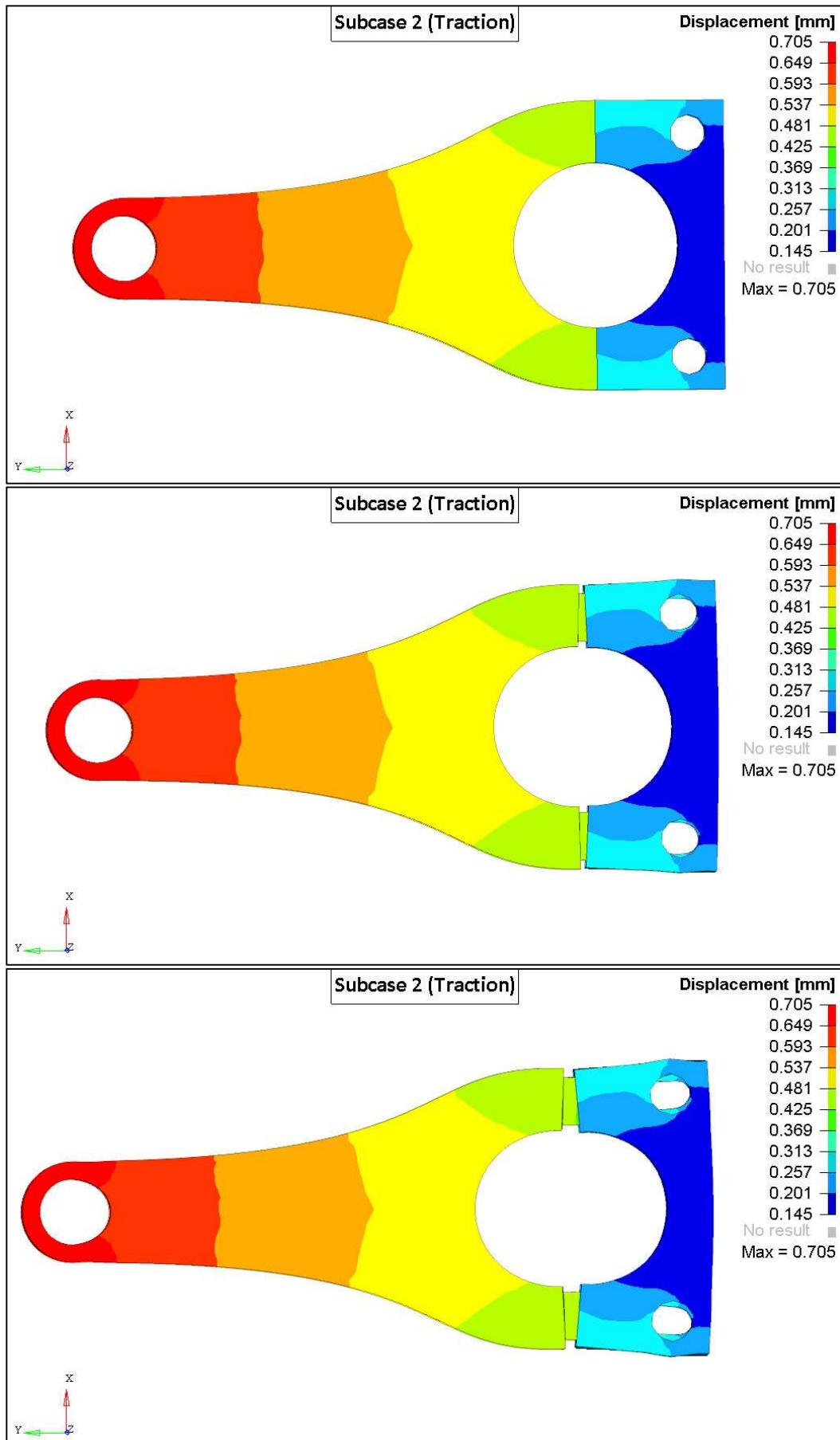


Figure 4-18 Traction: Enlarged Deformation

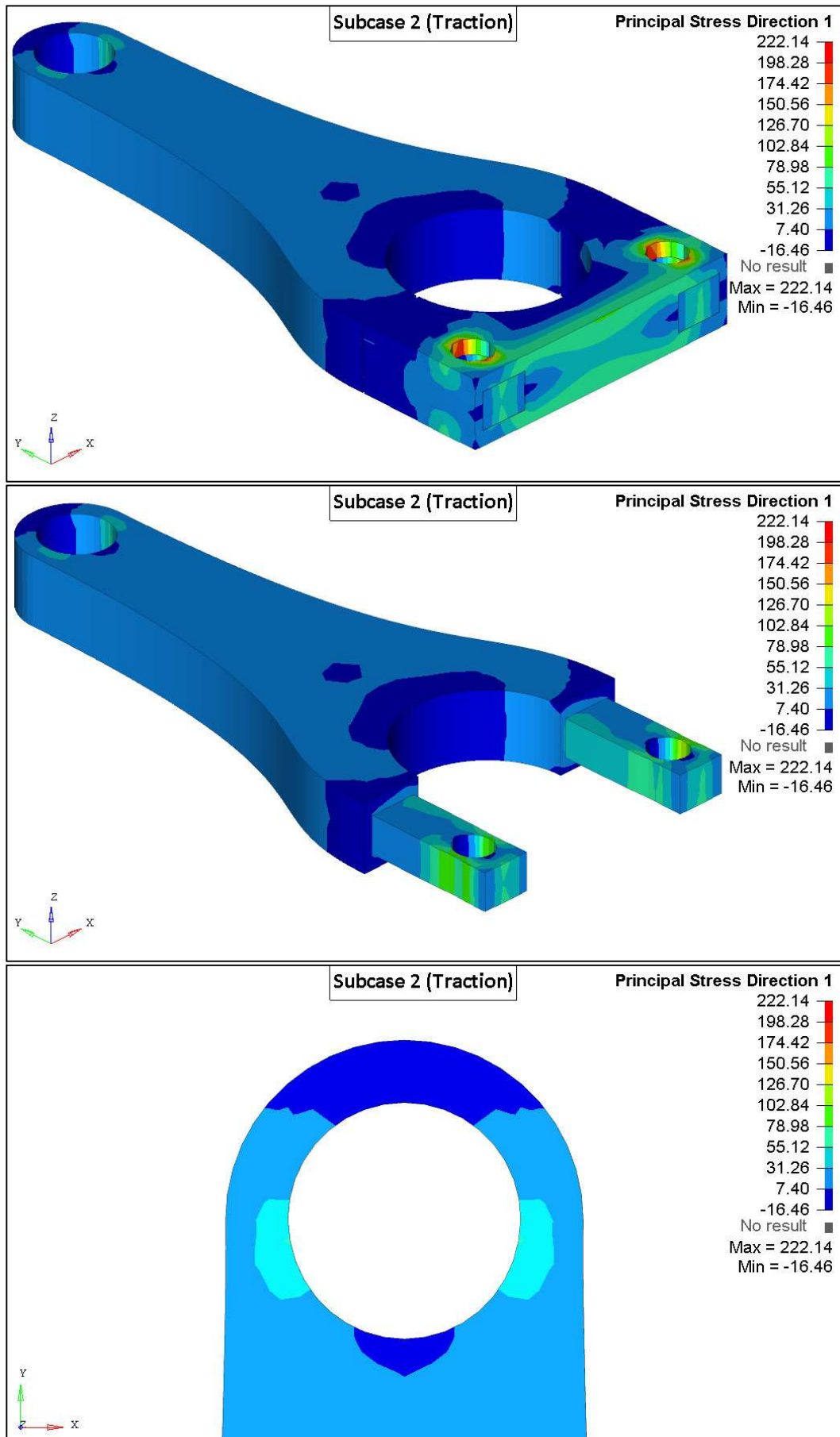


Figure 4-19 Traction: P1

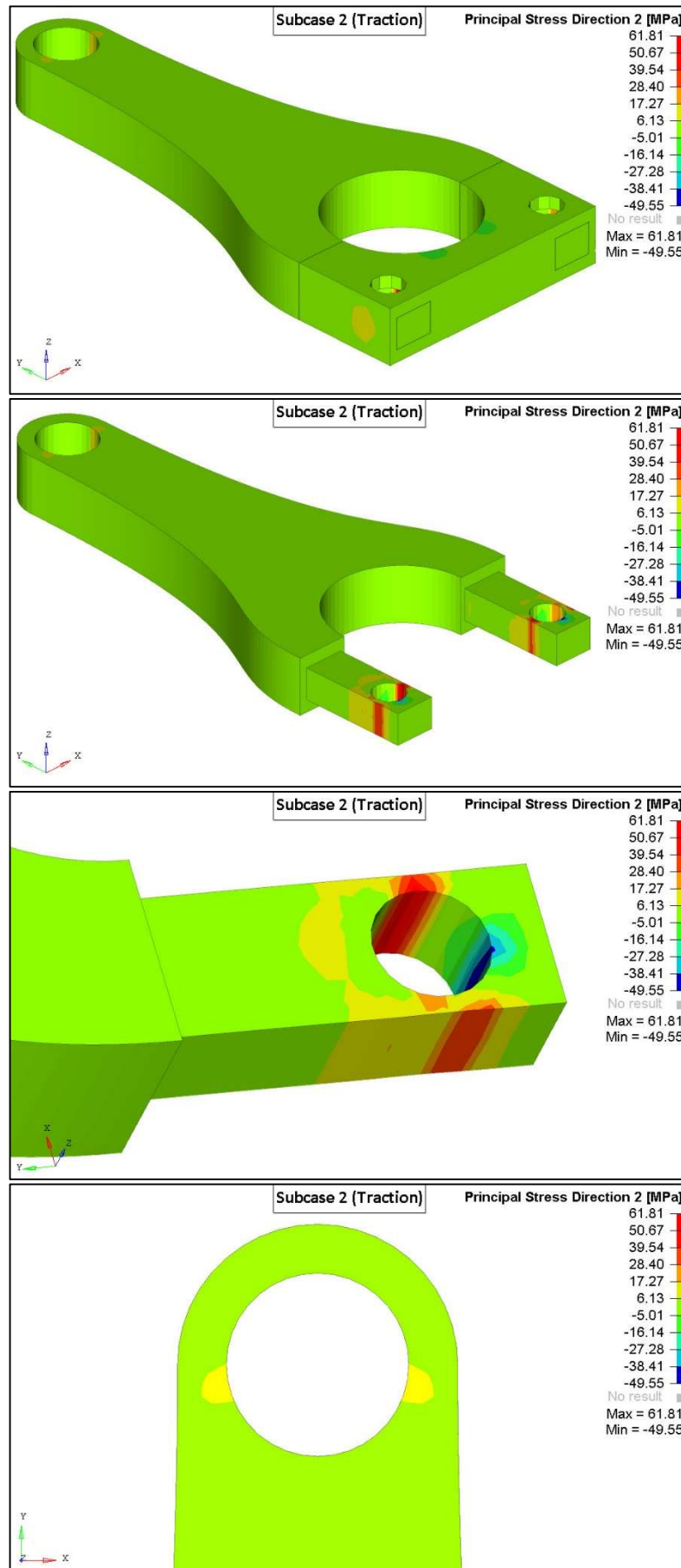


Figure 4-20 Traction: P2

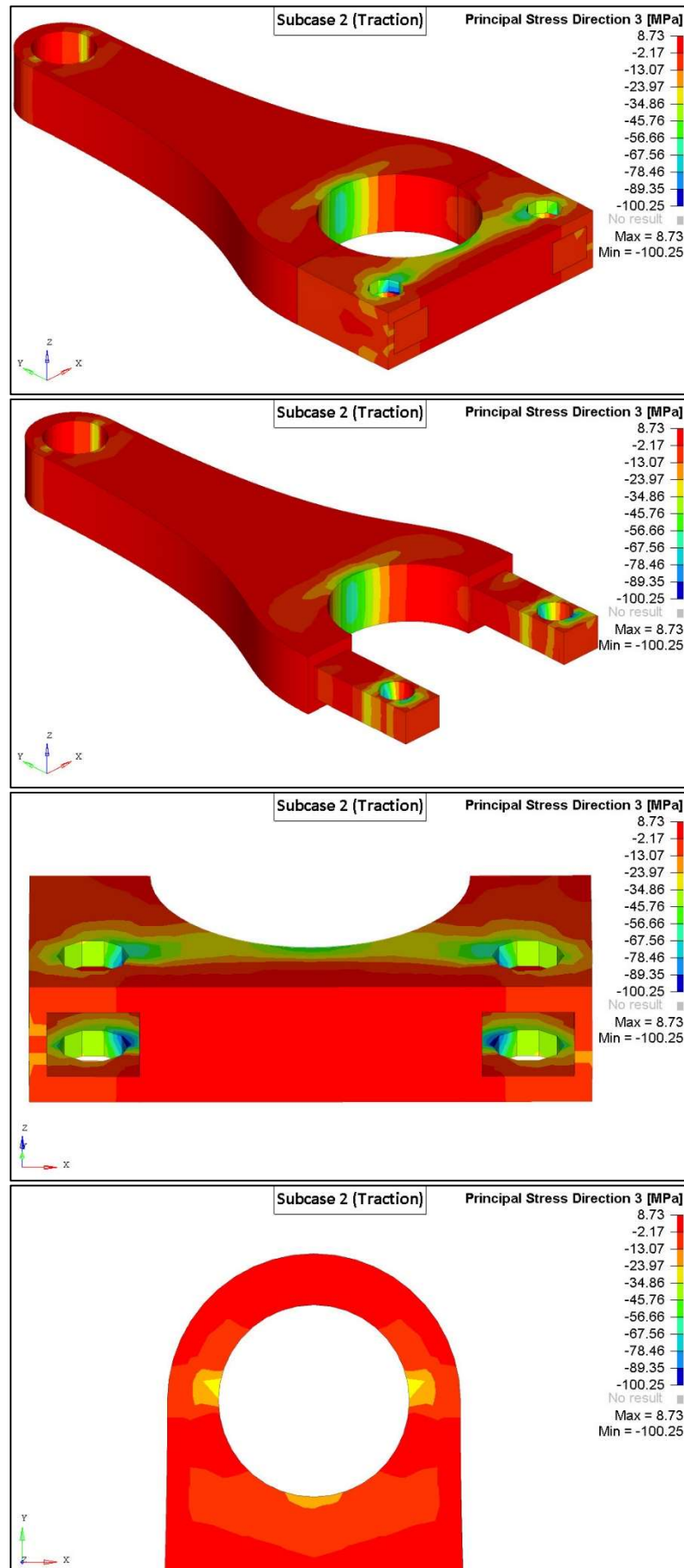


Figure 4-21 Traction: P3

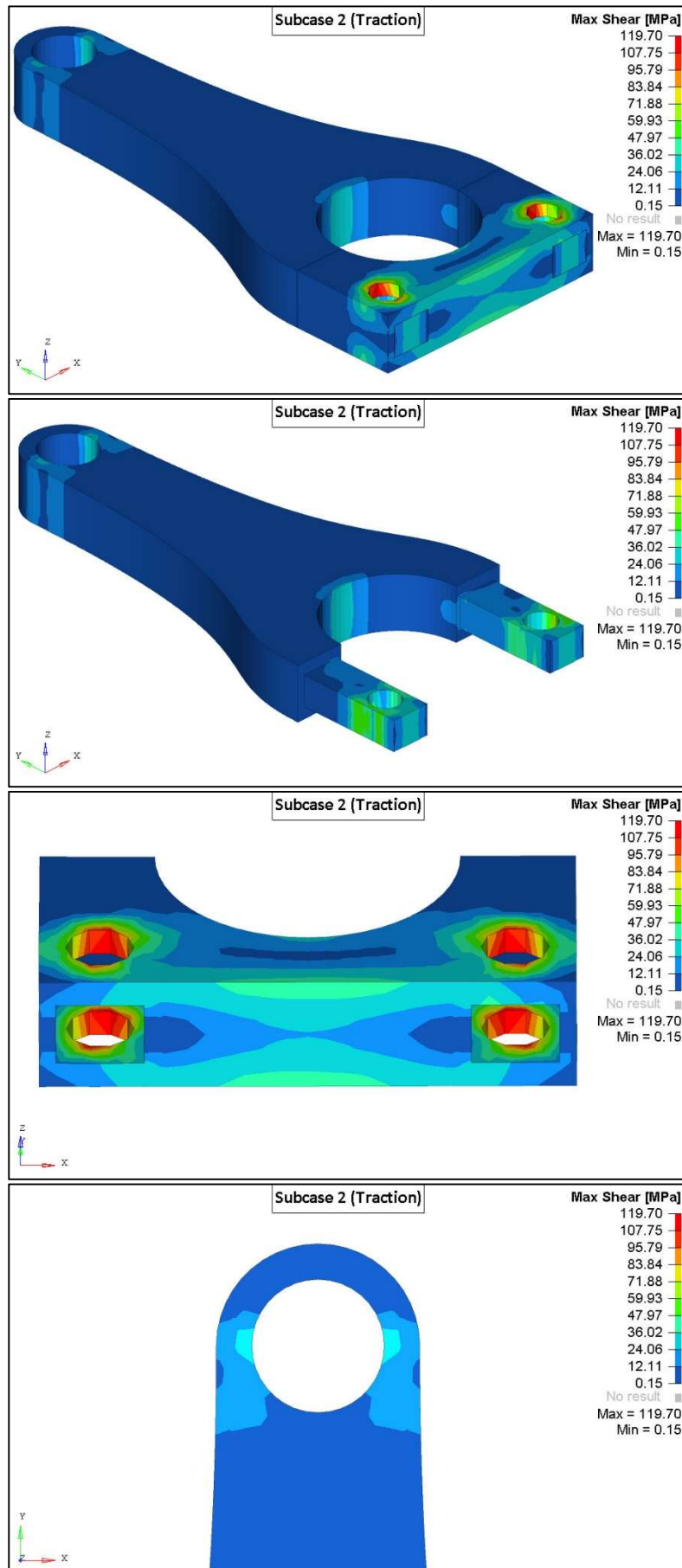


Figure 4-22 Traction: Max Shear

### 4.2.2 Buckling Load

It is shown the load that represents the compression. Same considerations about the usage of RBE2 as in the previous case.

The load step of the preload won't be explained again because it is equal than in the previous case, such as the constraints of both the load steps.

The  $F_{gas,max}$  is equal to 29814 N, while the  $F_{alt}$  in compression is equal to 3751 N: so the analysis was carried on considering the  $F_{gas}$ .

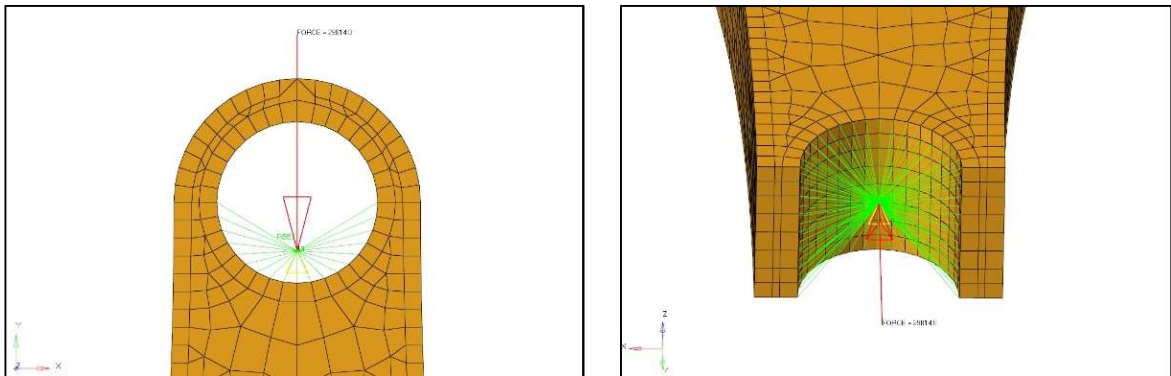


Figure 4-23 Buckling Load

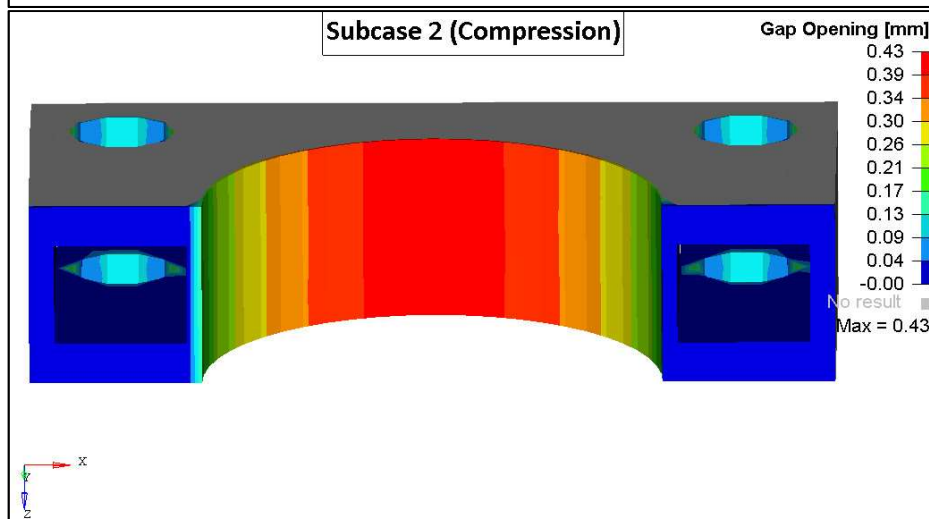
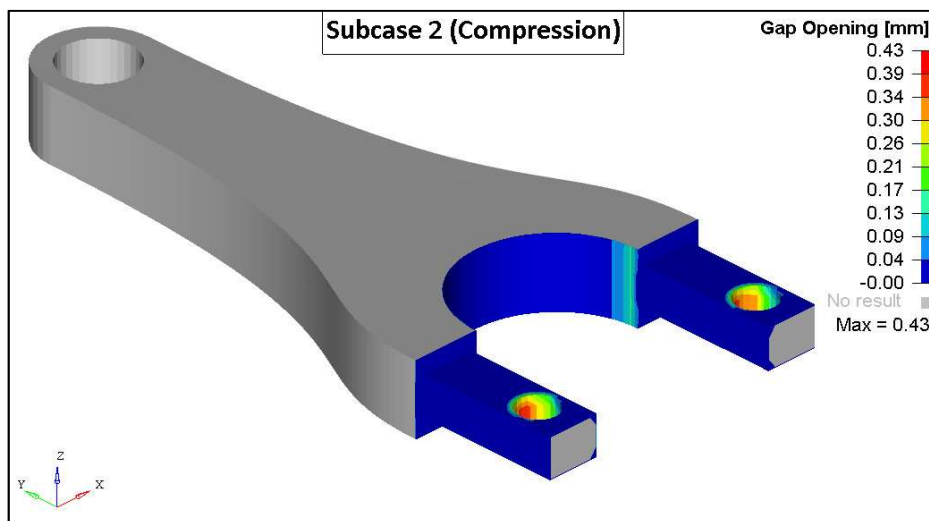


Figure 4-24 Compression: Gap Opening

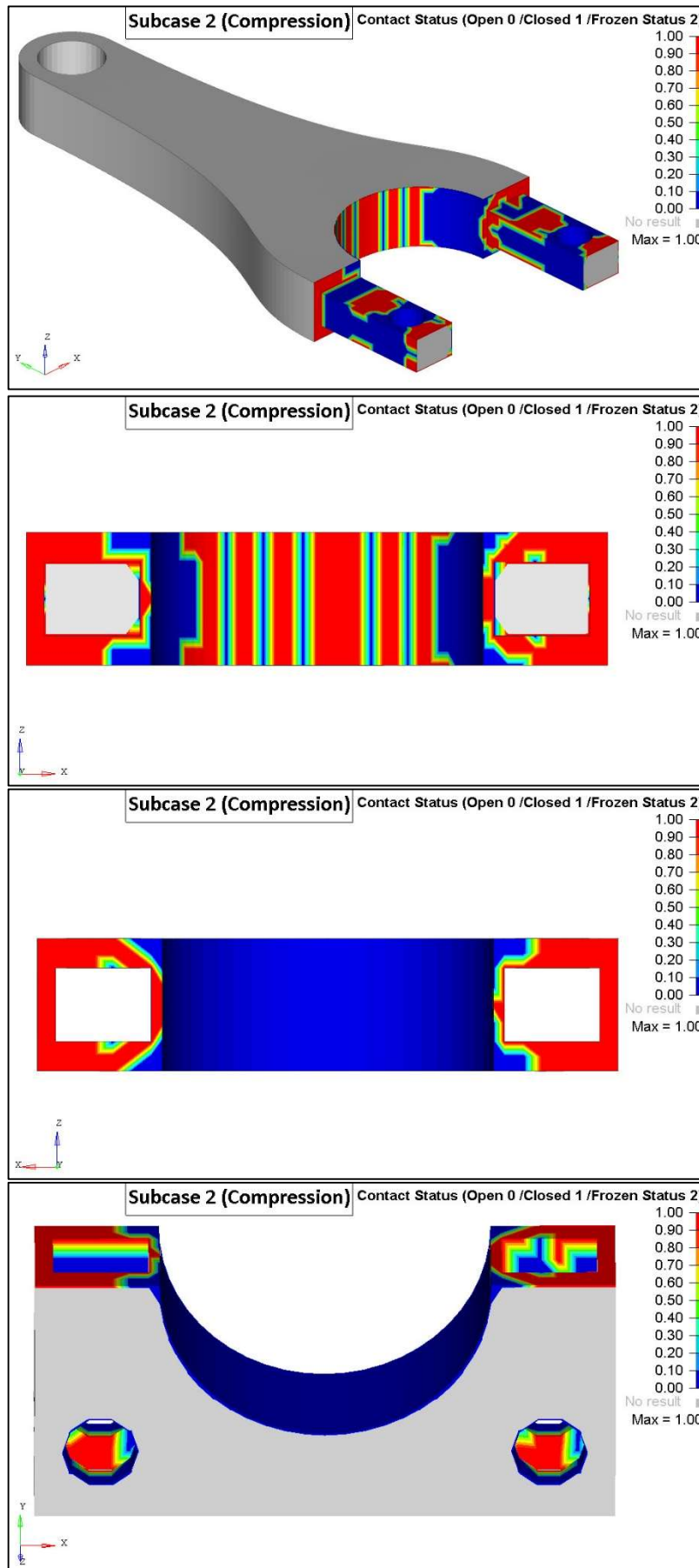


Figure 4-25 Compression: Contact Status

In the compression case, the gap opening is obviously less dangerous, but still present. The deformation is bigger than in the traction case: this is not strange in fact the carbon fibre works better in traction than in compression.

P1, P2, P3 and Max Shear magnitudes are like those of Traction case. For the reason above mentioned, this could be a more dangerous condition.

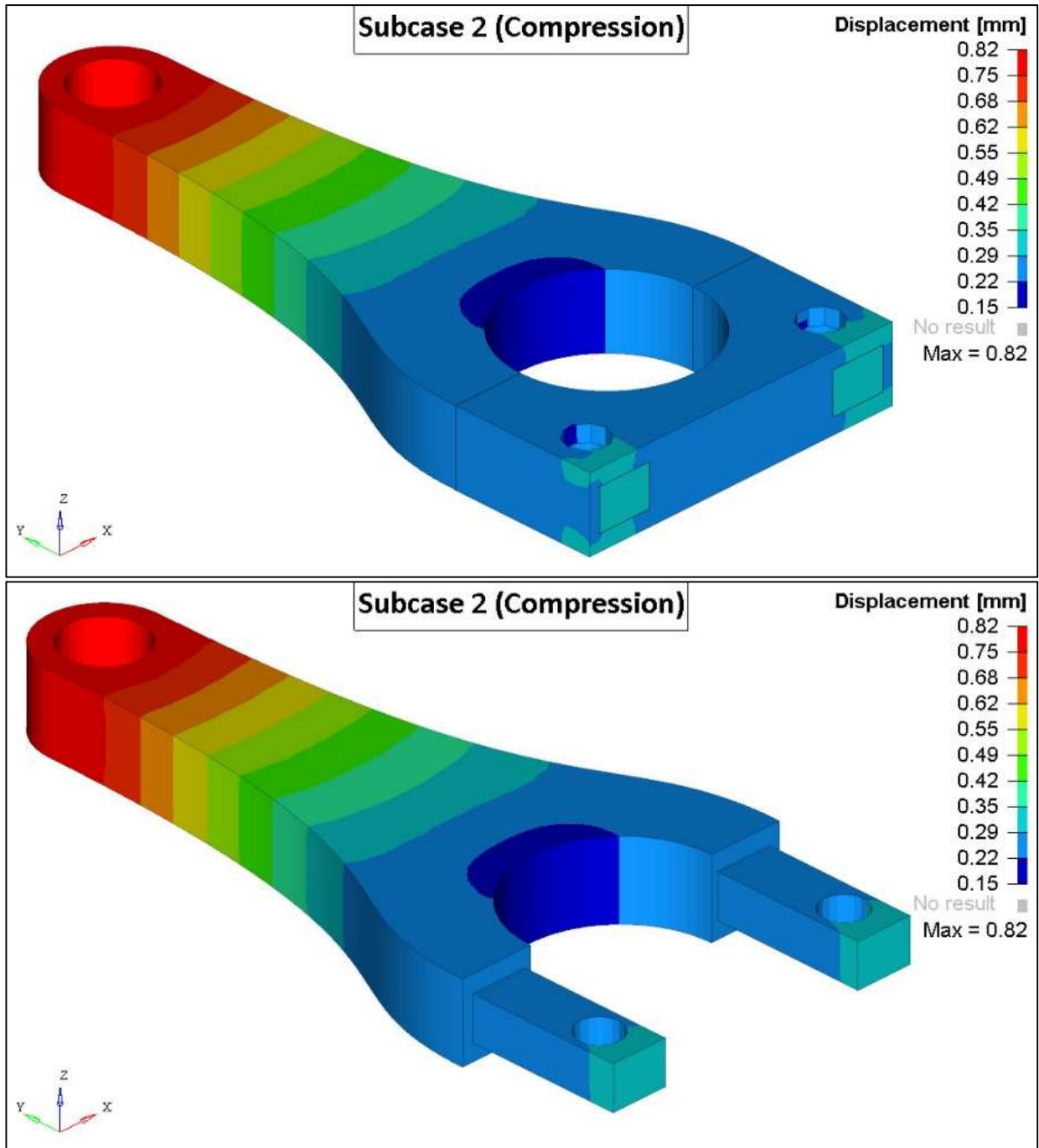


Figure 4-26 Compression: Displacement

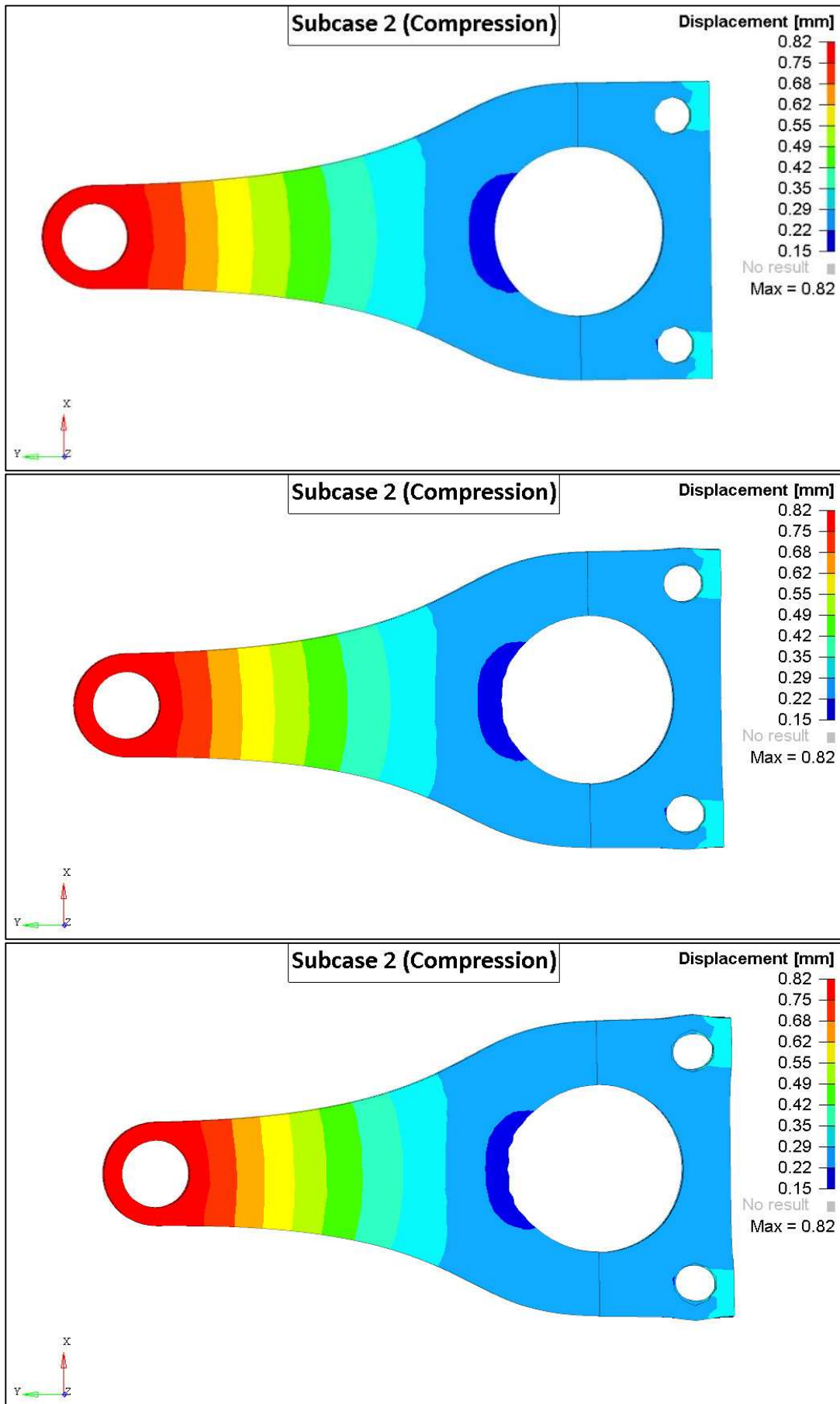


Figure 4-27 Compression: Enlarged Displacement

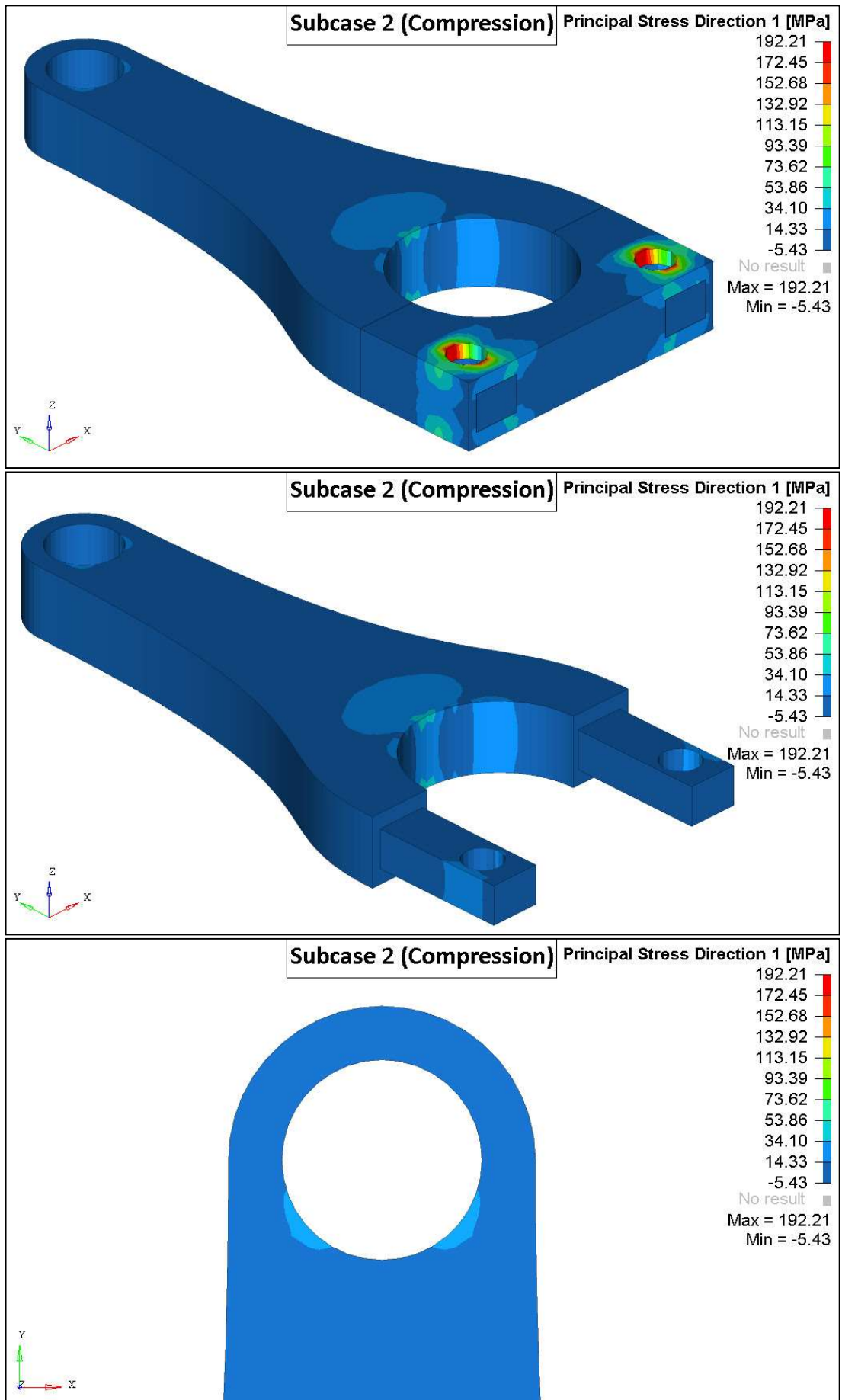


Figure 4-28 Compression: P1

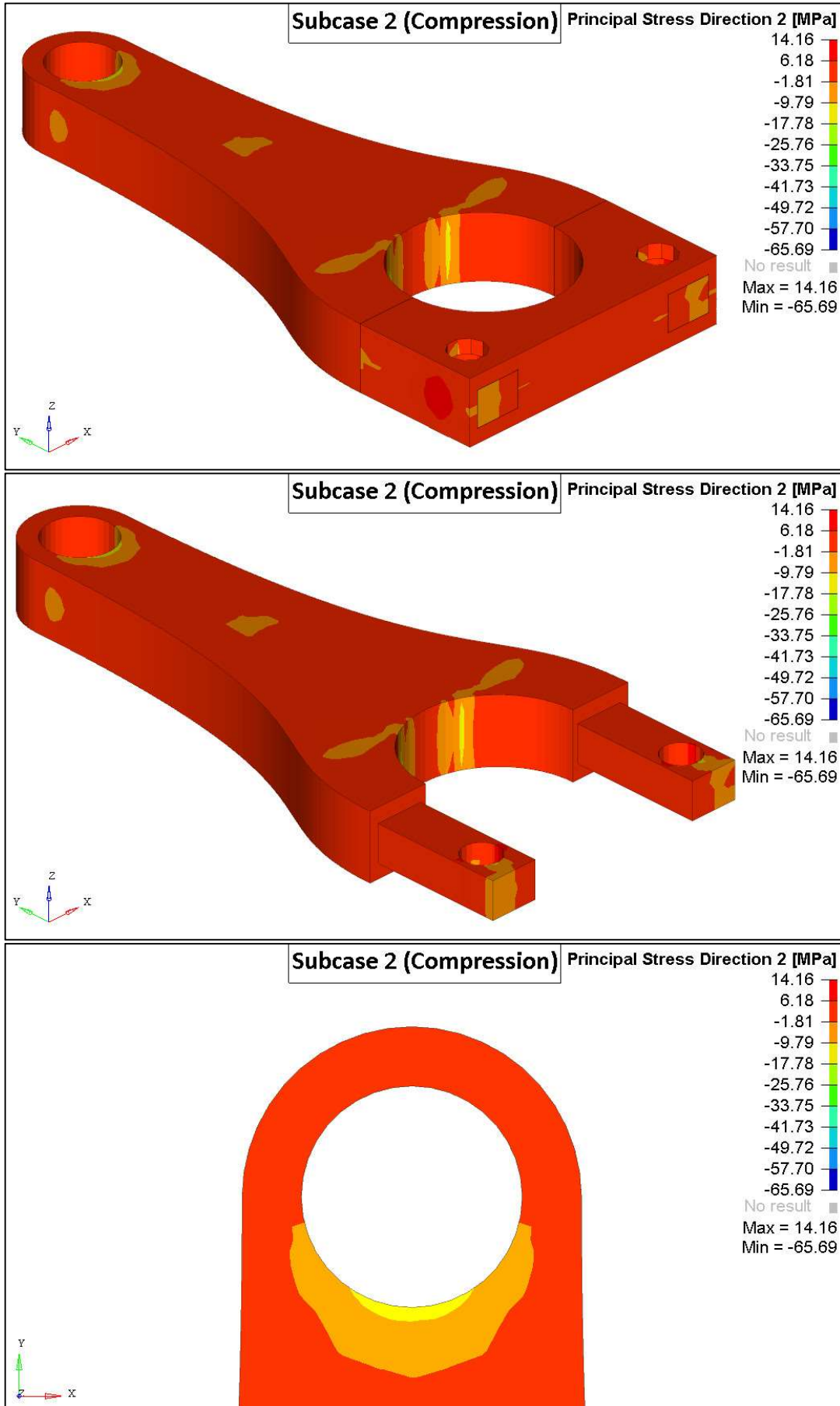


Figure 4-29 Compression: P2

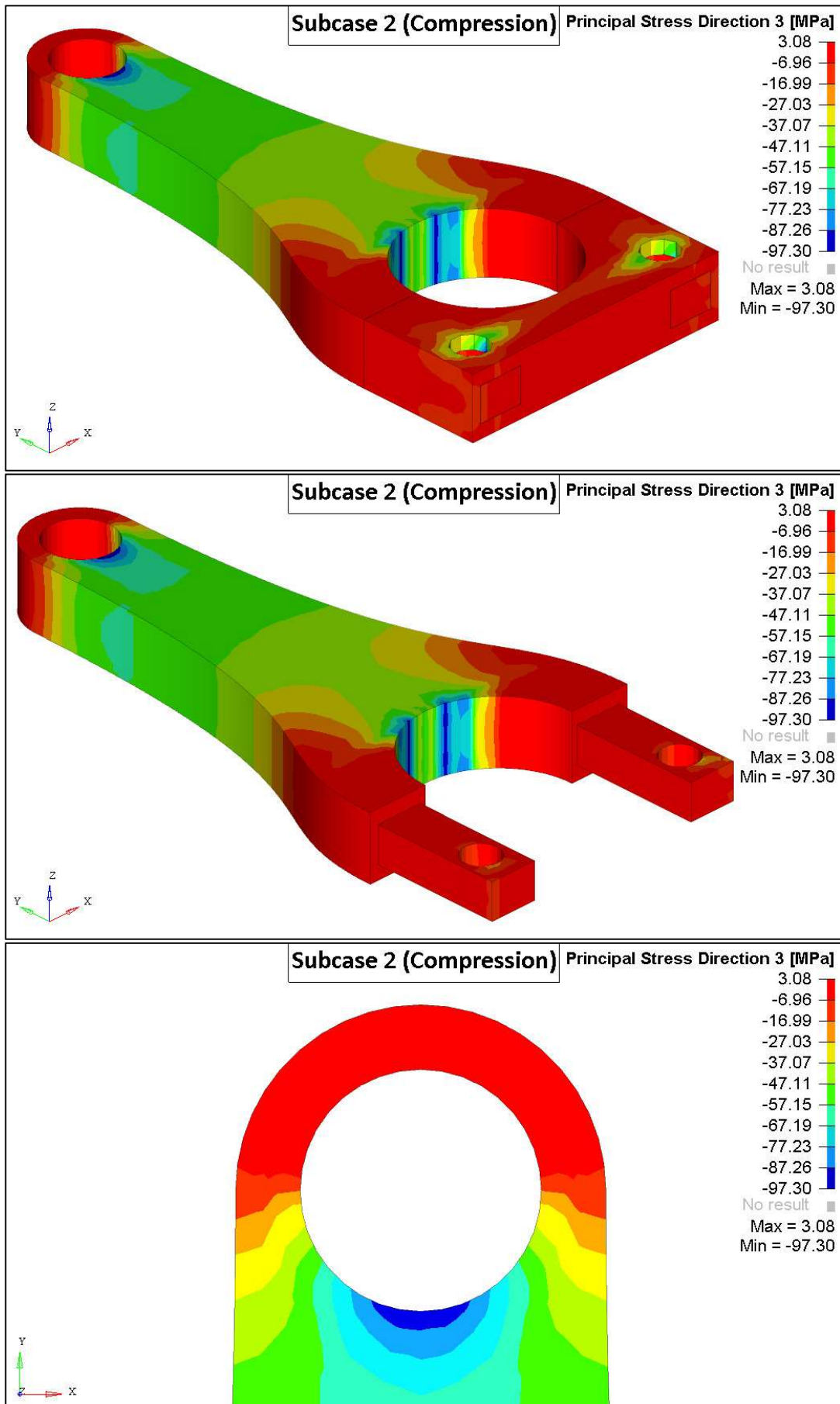


Figure 4-30 Compression: P3

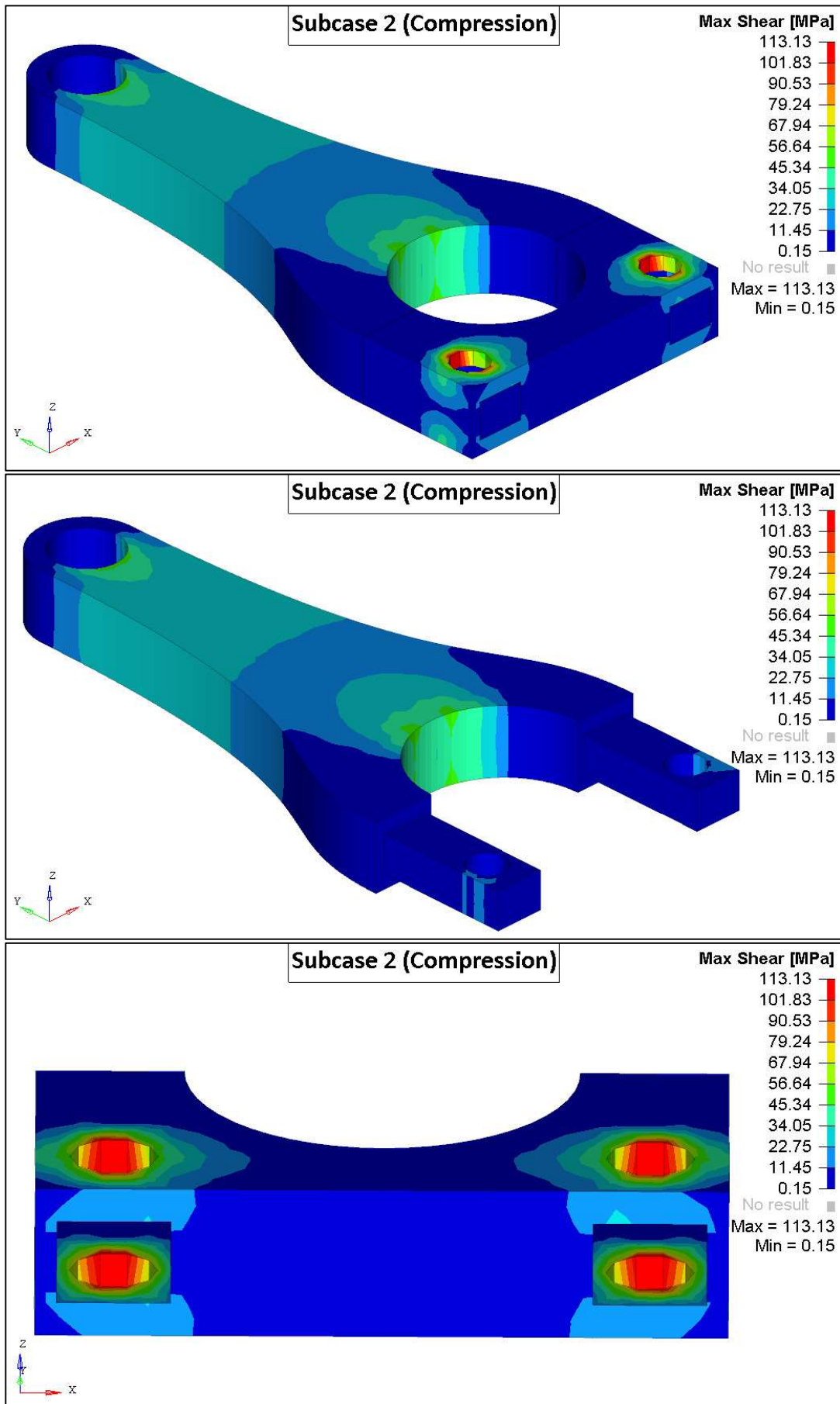


Figure 4-31 Compression: Max Shear

### 4.2.3 Bending Load

In this model, the constraints are the same than in other cases. The force is applied at one third of the distance between the small eye and the big eye.

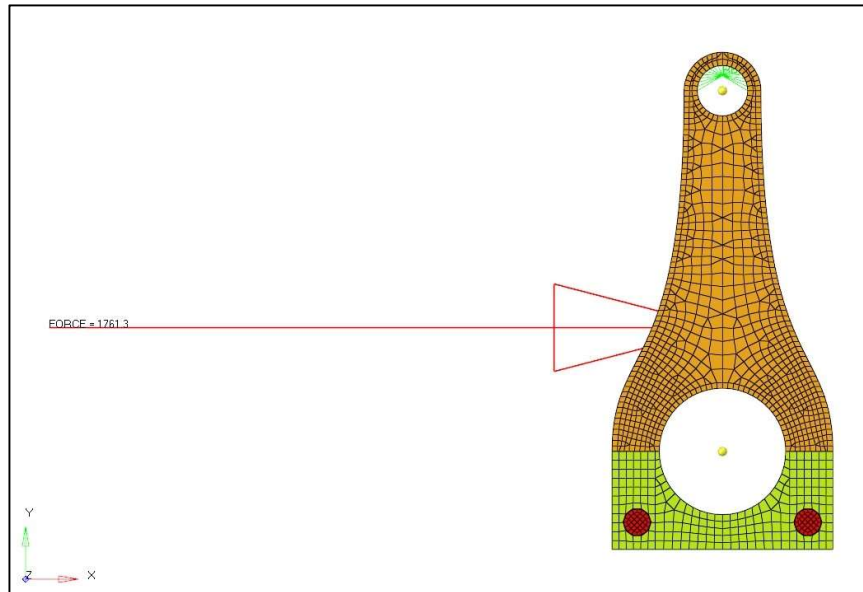


Figure 4-32 Whiplash Load

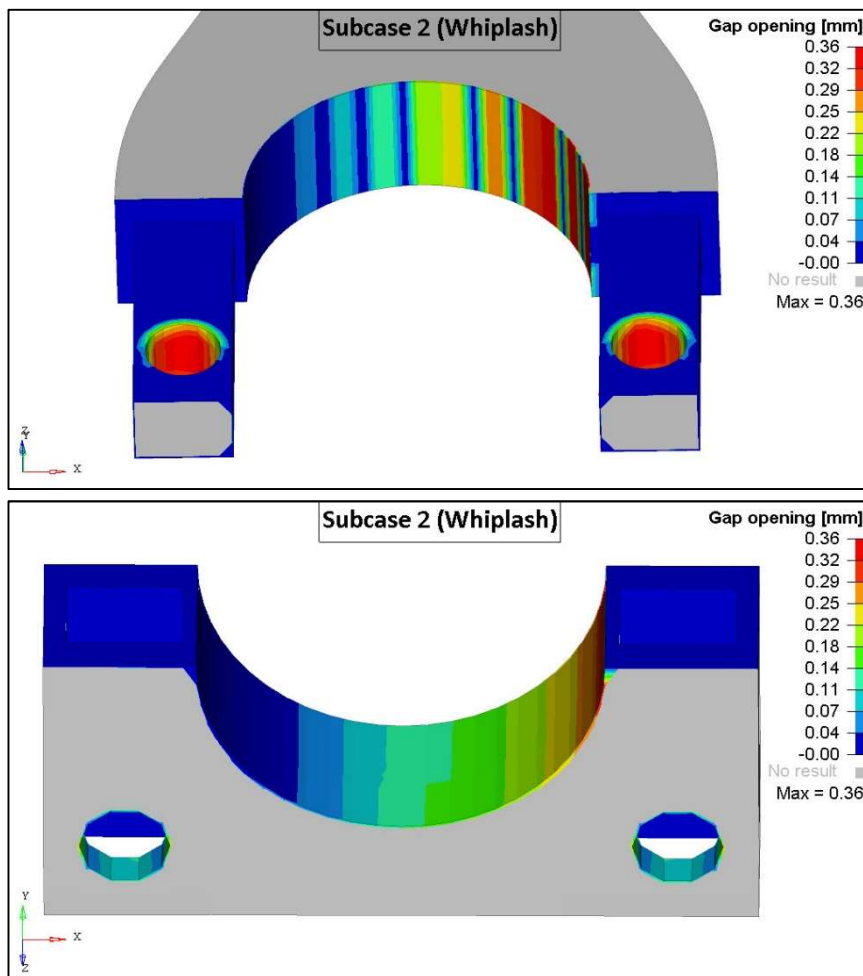


Figure 4-33 Whiplash: Gap Opening

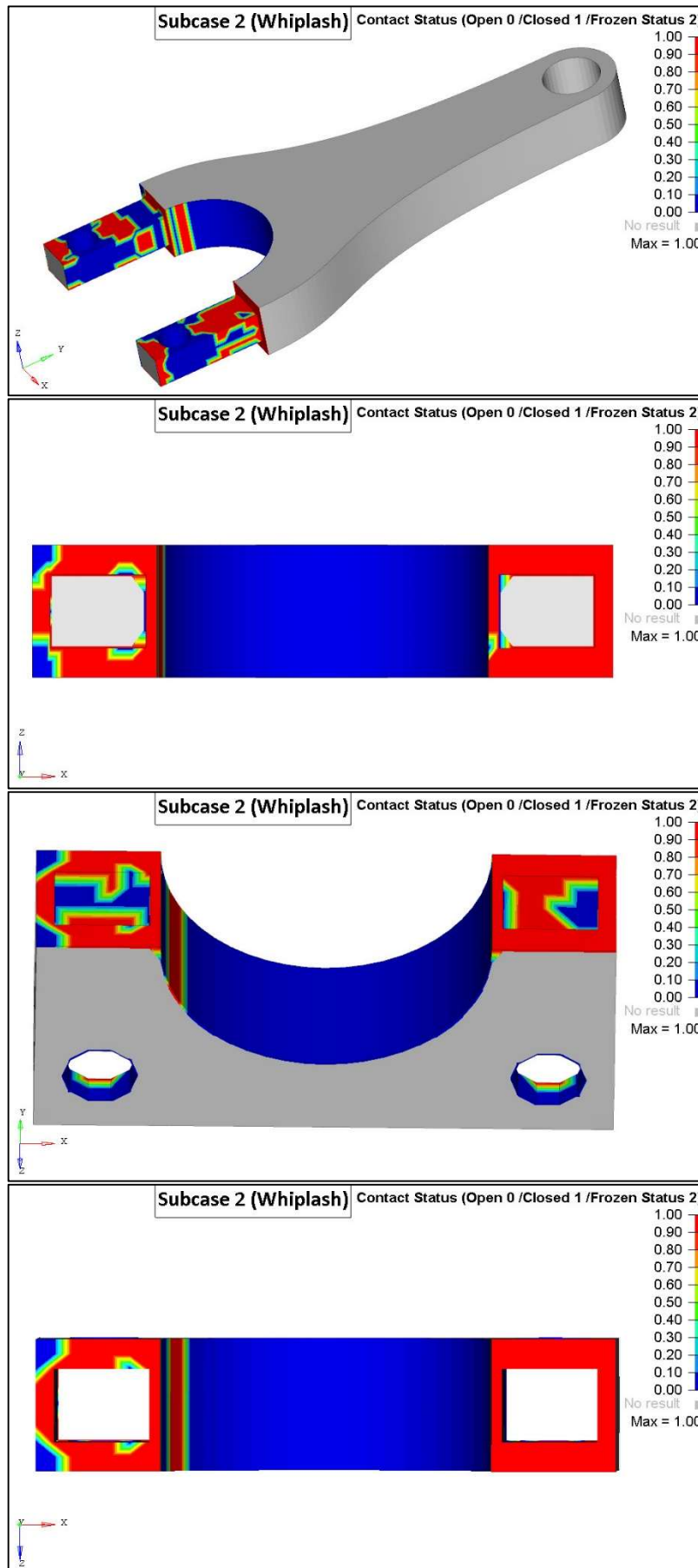


Figure 4-34 Whiplash: Contact Status

In this case, the contact is present in the surfaces between the cap and the stem, while is not guarantee between the rod and the crankshaft. This problem is present in all the load analysed and it is mainly linked to the preload given through the misalignment of the pin holes, as said in the previous pages.

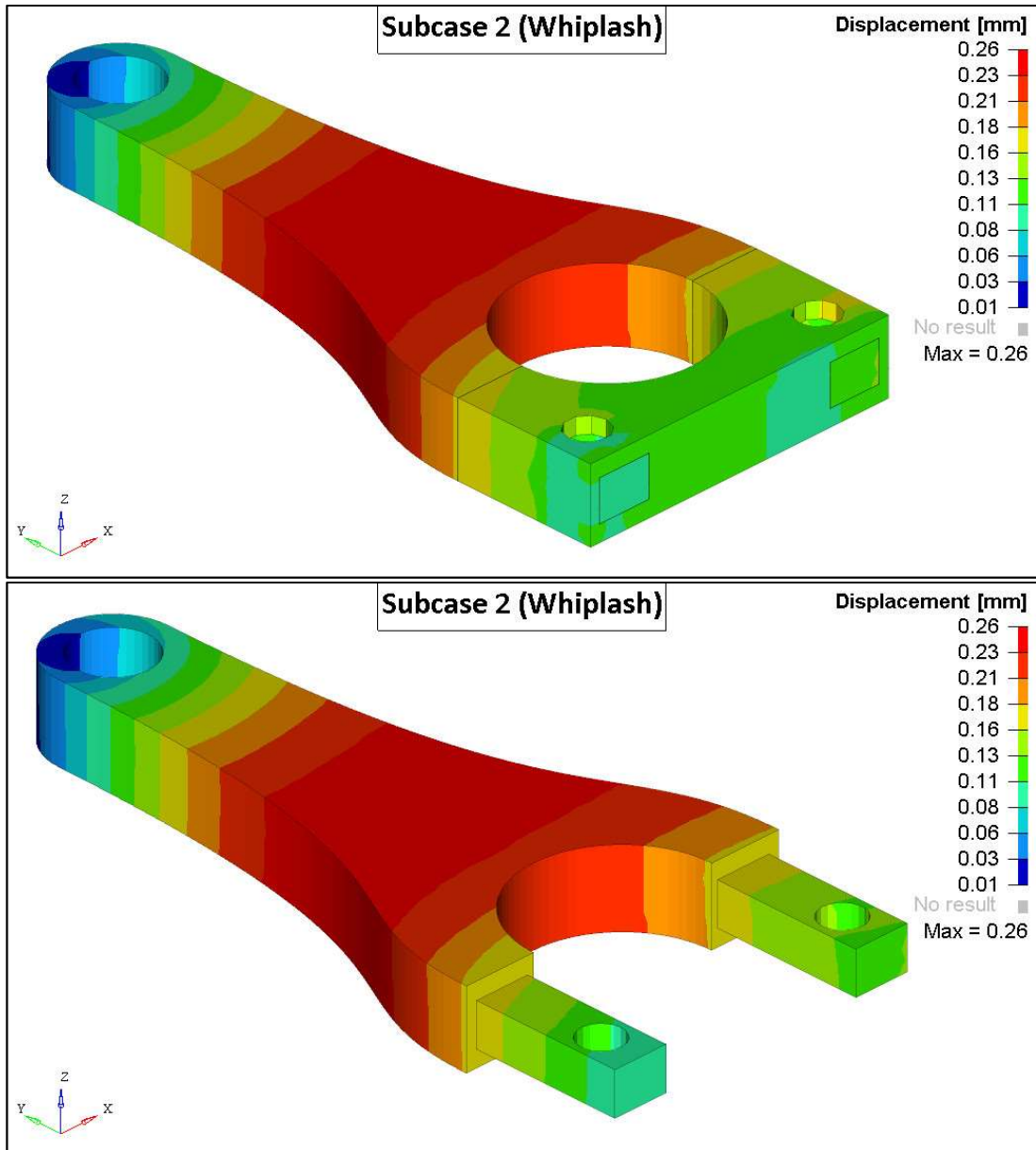


Figure 4-35 Whiplash: Displacement

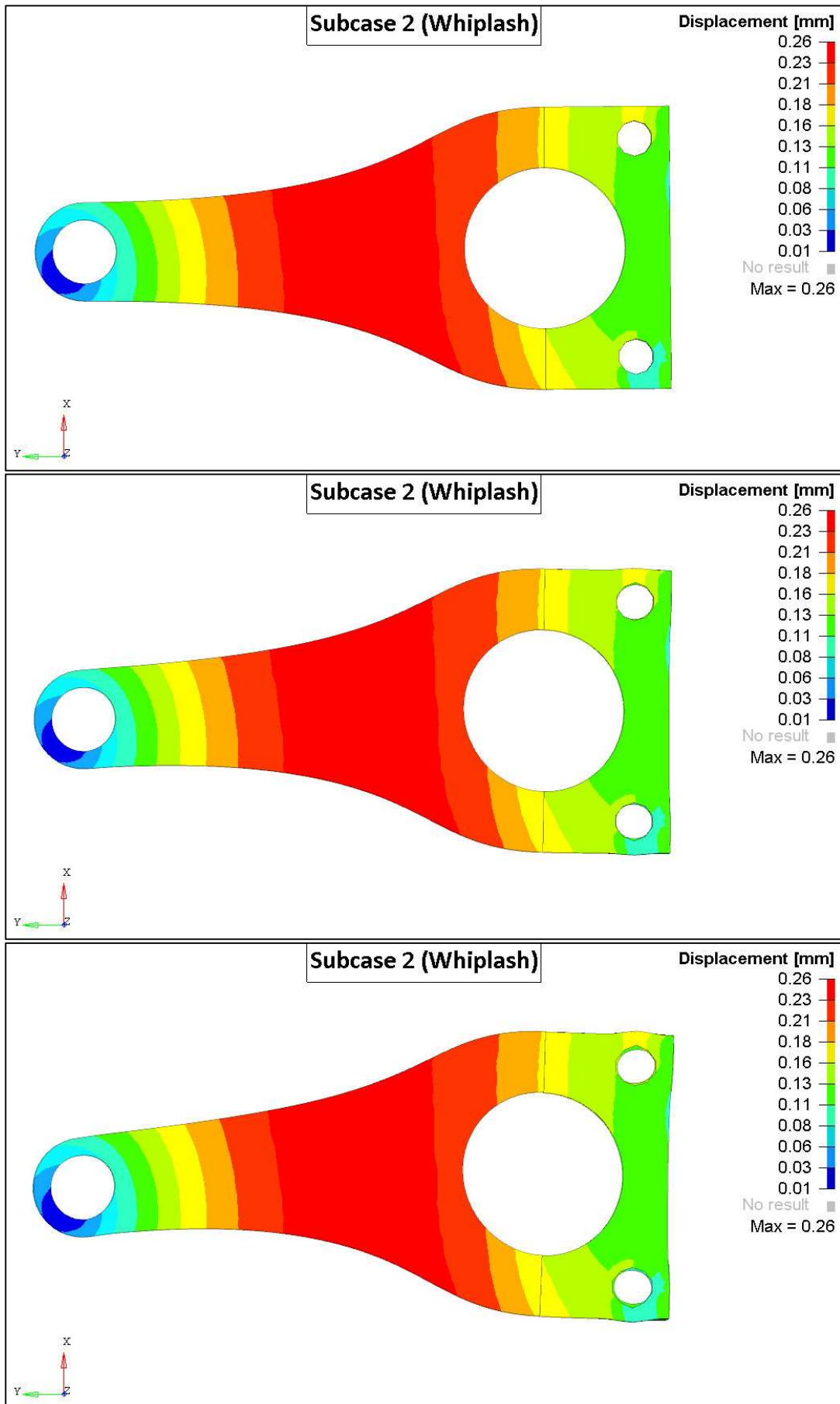


Figure 4-36 Whiplash: Enlarged Deformation

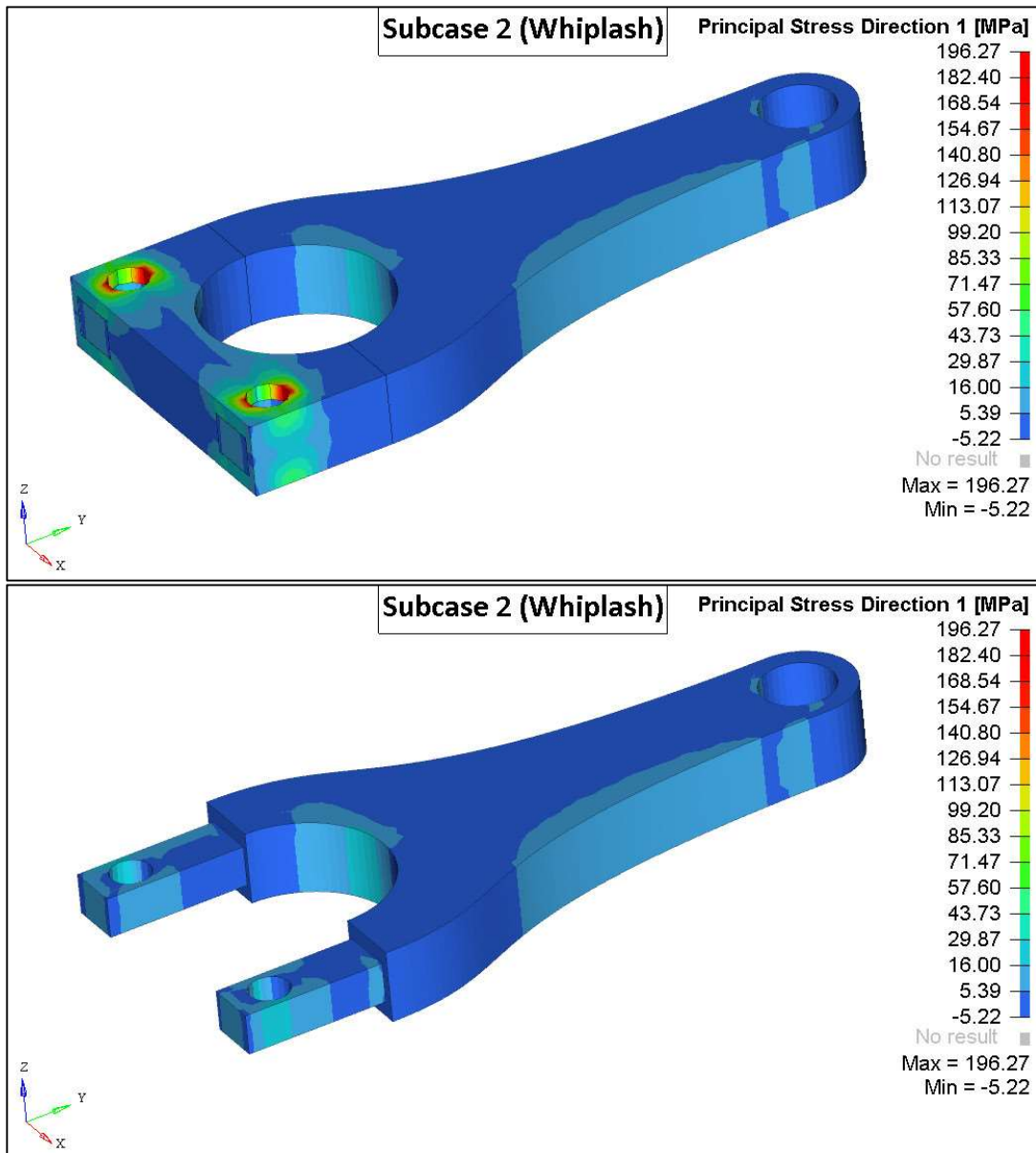


Figure 4-37 Whiplash: P1

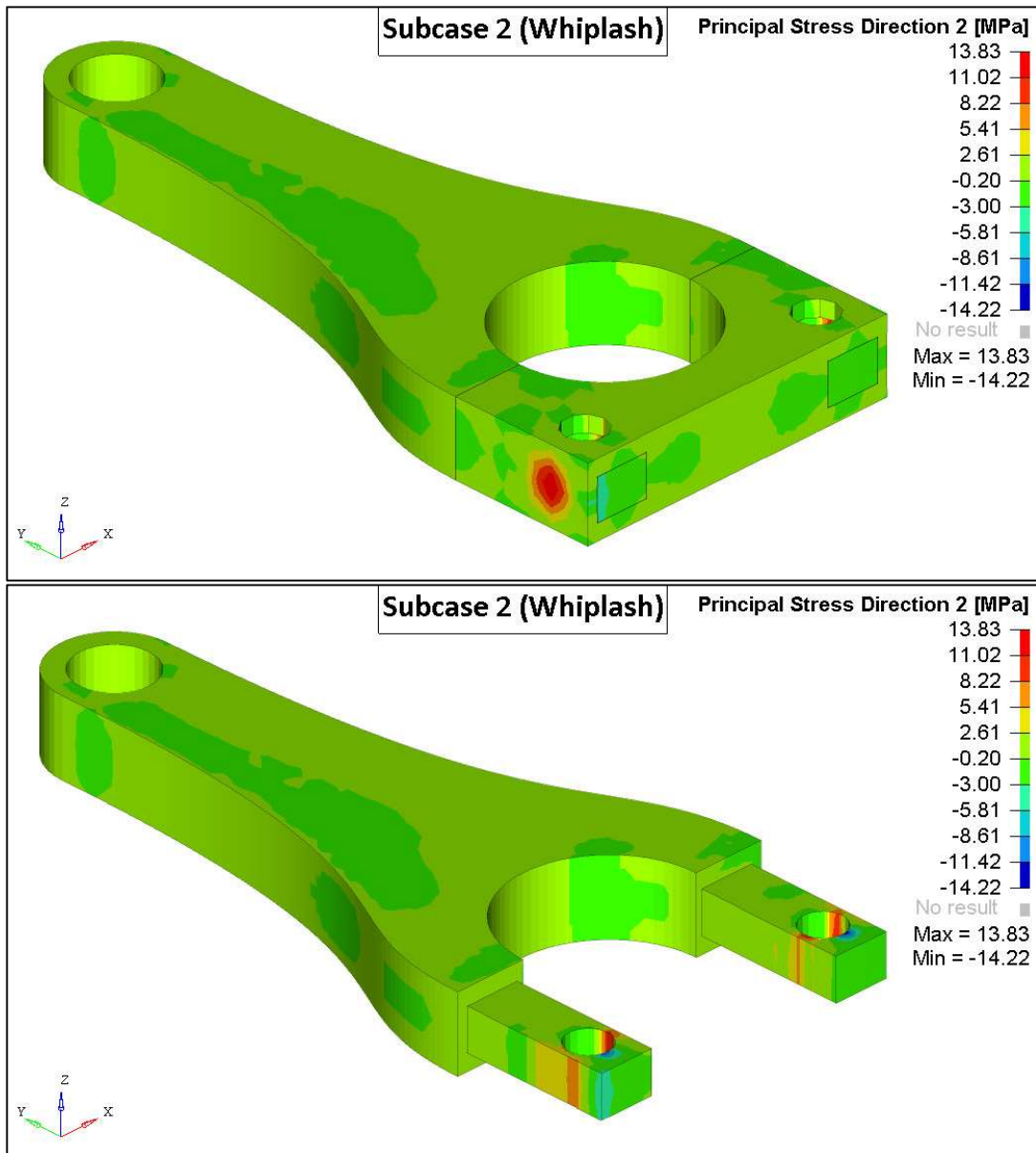


Figure 4-38 Whiplash: P2

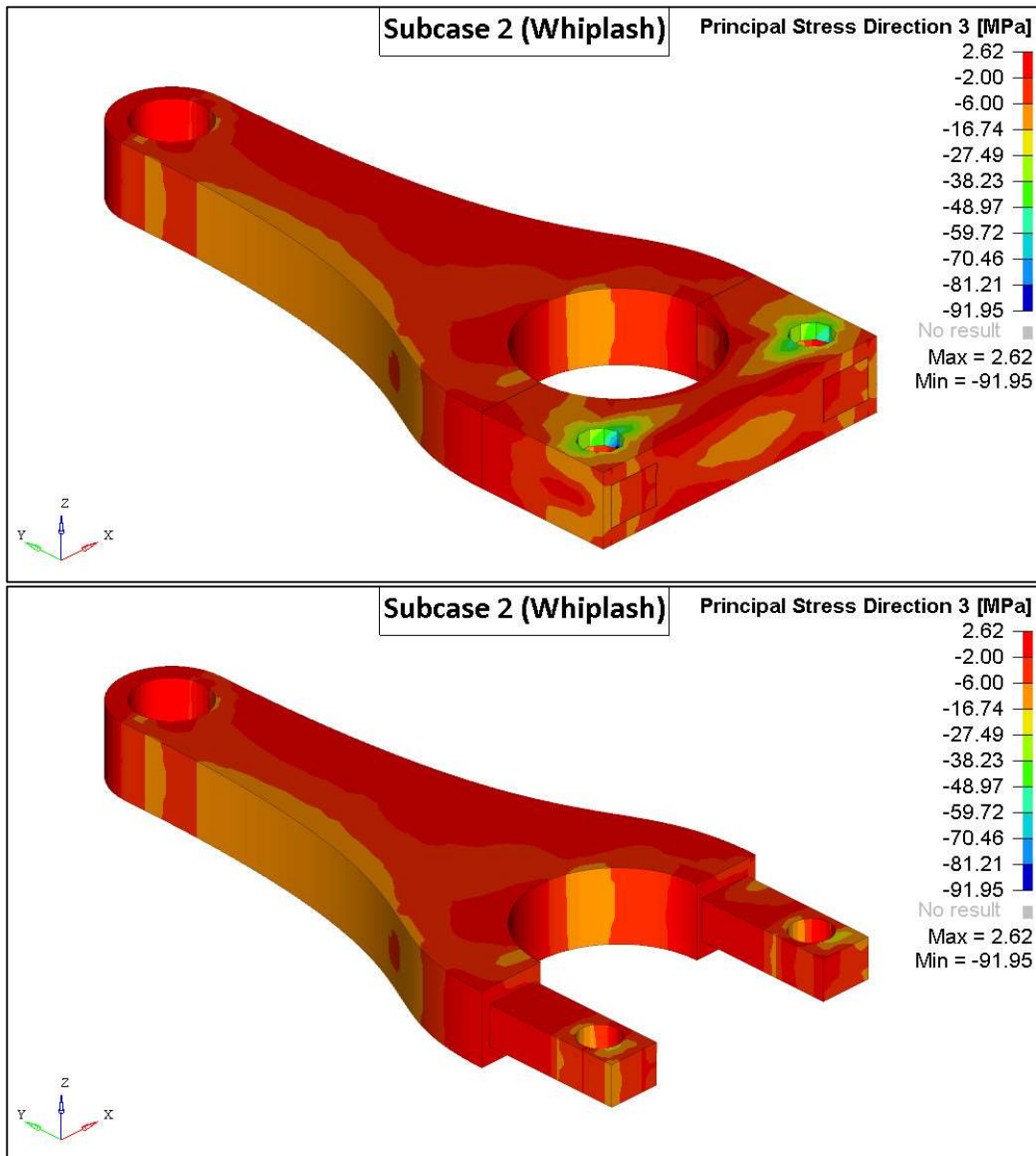


Figure 4-39 Whiplash: P3

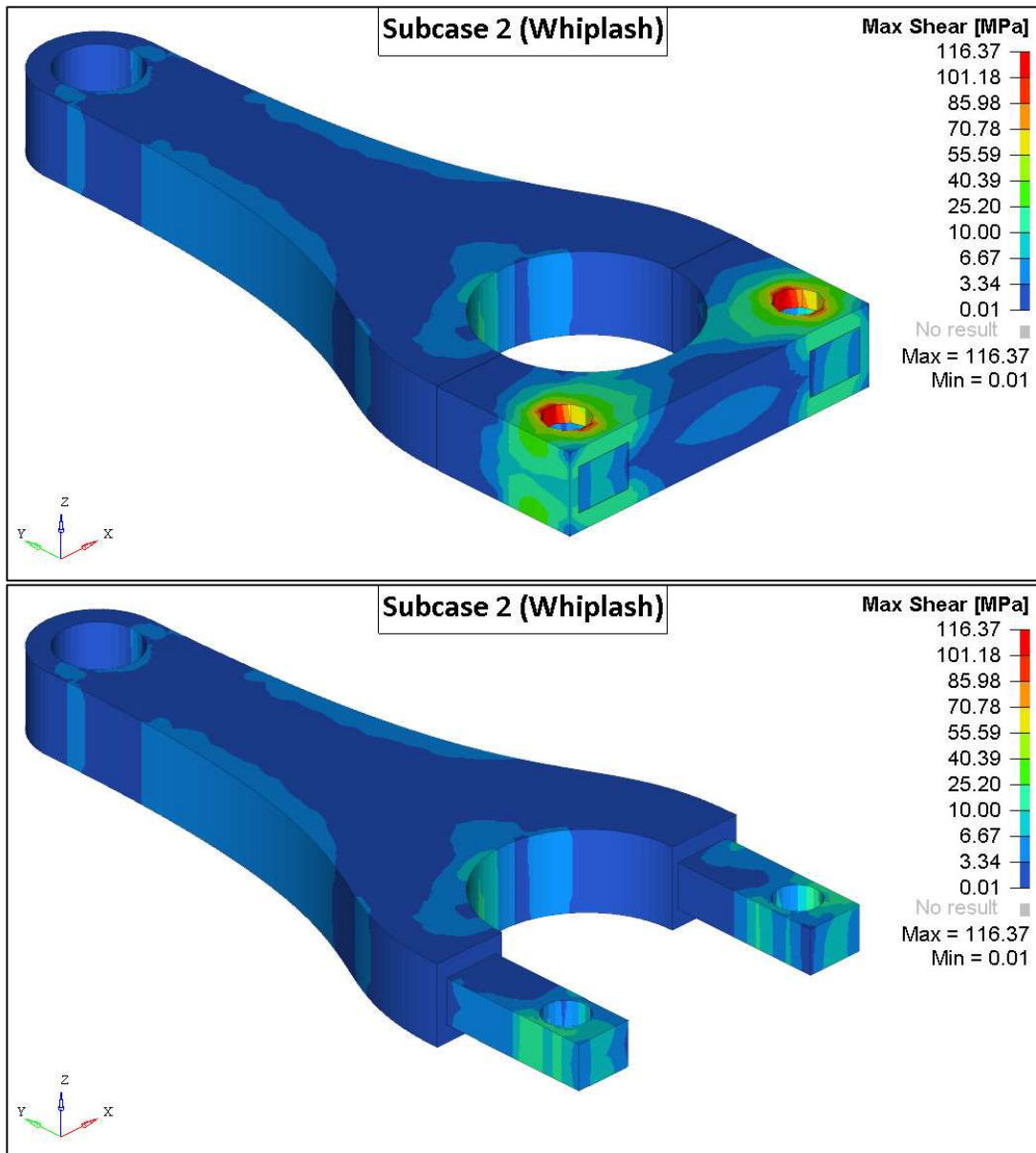


Figure 4-40 Whiplash: Max Shear

The stress distribution confirms the hypothesis about the need of an appropriate layer distribution of carbon fibres around the pin holes, the small and big eye and on the lateral surface of the stem. Further explanations in the next paragraph.

### 4.3 Future development

From a software point of view, a further advancement is conditioned by the release of the new HyperMesh 2019, which should contain all that features above mentioned in the PCOMPLS paragraph.

Regarding the layering method, an optimization of the different plies can be subject of a future thesis. This project aim was to introduce the PCOMPLS elements and to lighten an engine component. These objectives were partially reached, because it wasn't possible to use PCOMPLS reliably. The orientation of the fibres wasn't optimized, but only chosen an orthotropic material. The results of this project represent a "launch pad" for future thesis about composite components simulation on HyperMesh and Optistruct.

The lightening of the engine wasn't faced in a complete way. Only the wrist pin and the connecting rod were analysed. The weight reduction of the connecting rod and of the wrist pin should be accompanied by a lightening of the other engine components, such as the crankshaft, crankwebs and crankcase. This overall lightening would bring to a substantial benefit.

From an experimental point of view, a thesis focused on the test of the composite material UD PEI-AS4 would be recommended to validate the software results and the mechanical characteristics of the material, too.

Regarding the material, it would be positive to evaluate also the use of alternative composite material with a better rub resistance, such as the Kevlar, on the layer of the rod and the pin where they are in contact with the bushing. In fact, the oil layer should be always present, but in any case, this solution could give a better safety coefficient. Another benefit could be the possibility to add circumferential sheets of carbon fibre around the pin holes: in such a way the carbon fibre can react more efficiently to the load.

Those could be some example of layer diversification:

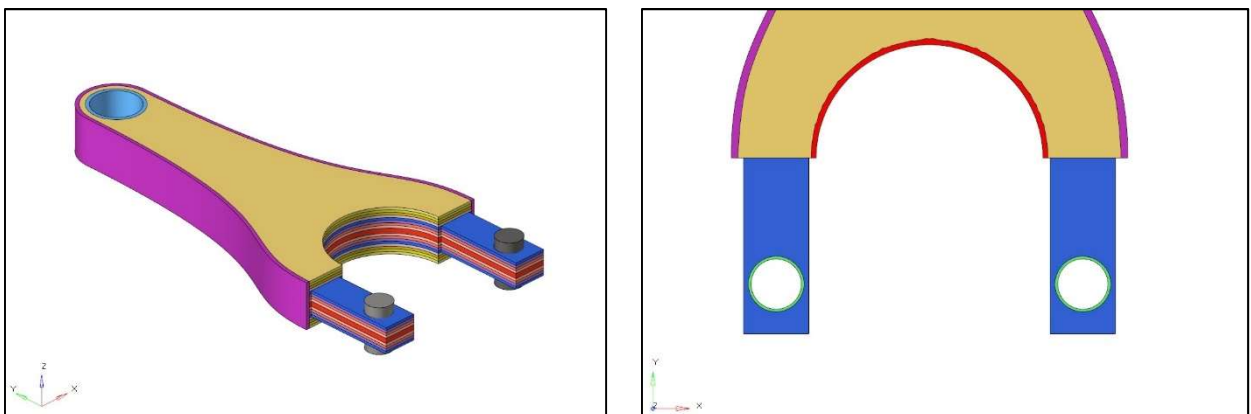


Figure 4-41 Example of Layer Diversification

#### 4.4 *Alternative model*

Below, an alternative model is shown. The legs of the stem are larger: this solution allows to gain space to add layers of material around the pin holes, which are the most stressed zones.

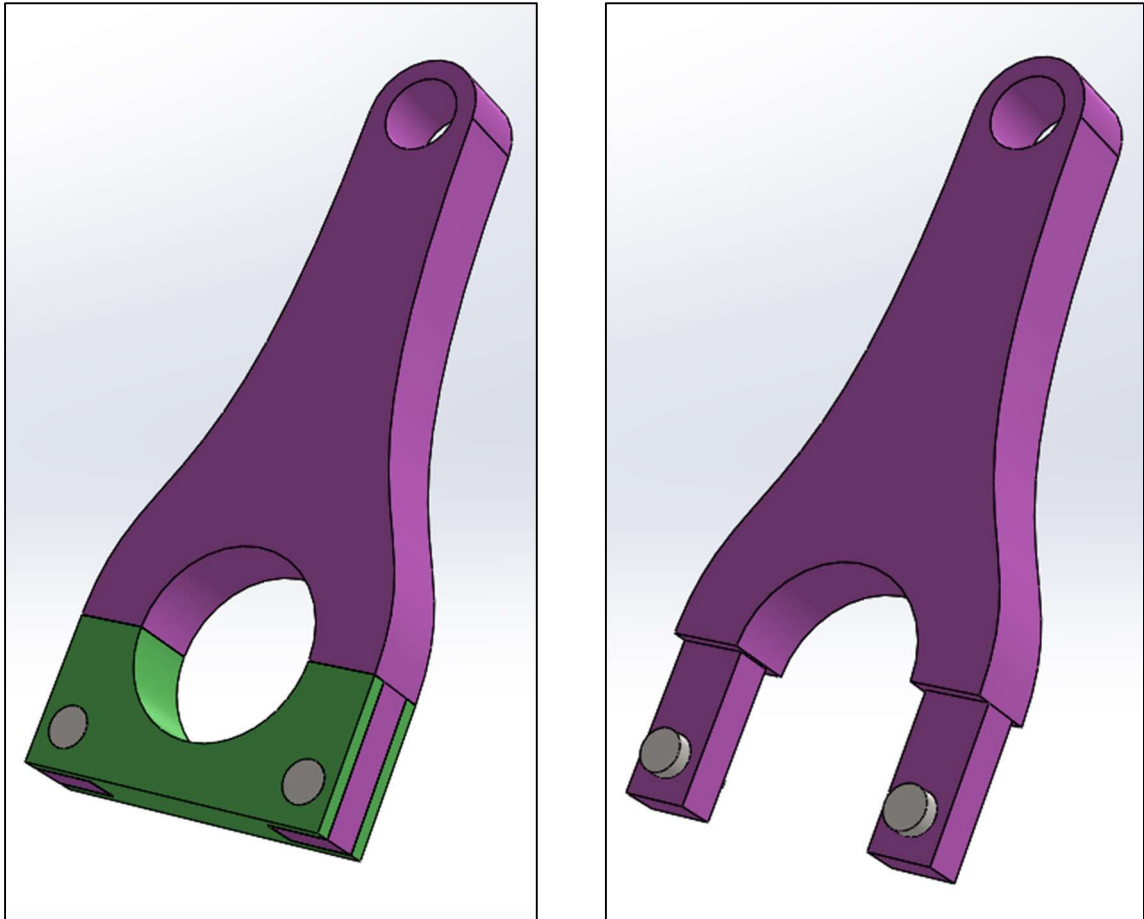


Figure 4-42 *Alternative Model*

Another solution could be to assign the preload between cap and stem through a pin with the shape of a cam.

## I. Bibliography

Cristiana Delprete, *Powertrain Component Design, Educational material*,  
Available: <https://didattica.polito.it/>

Altair Engineering. Available: <http://www.altair.com>.

Altair Connect. Available: <https://connect.altair.com/>

Altair Forum. Available: <https://forum.altair.com/>

Altair University released: 1<sup>st</sup> edition 05/2018, *Academic Program: Introduction to Practical Aspects of Composites*

Shuguang Li, Elena Sitnikova, Yuning Liang, Abdul-Salam Kaddour, August 2017, *The Tsai-Wu failure criterion rationalised in the context of UD composites*,  
Available: [www.elsevier.com/locate/compositesa](http://www.elsevier.com/locate/compositesa)

*Six-Sided Solid Element Connection - Figure 2. CHEXA Element R, S, and T Vectors*,  
Available: <https://knowledge.autodesk.com/support/nastran>

Yijing Li and Jernej Barbič, *Stable Orthotropic Materials*, Vladlen Koltun and Eftychios Sifakis

Giuseppe La Placa, *Design of engine components with thermoplastic composite material*,  
2019

Ömer Faruk Kale, *Design and Analysis of Composite Conrod Using Finite Element Method*,  
2019